AAEC/E351

AUSTRALIAN ATOMIC ENERGY COMMISSION

RESEARCH ESTABLISHMENT

LUCAS HEIGHTS

THE CALCULATION OF FULLY DEVELOPED TURBULENT AND LAMINAR SINGLE PHASE FLOW IN FOUR-ROD SUBCHANNELS

by

J. D. HOOPER

September 1975

ISBN 0 642 99684 9

AUSTRALIAN ATOMIC ENERGY COMMISSION
RESEARCH ESTABLISHMENT
LUCAS HEIGHTS

THE CALCULATION OF FULLY DEVELOPED TURBULENT AND LAMINAR SINGLE PHASE FLOW IN FOUR-ROD SUBCHANNELS

by

J.D. HOOPER

ABSTRACT

A numerical model of a turbulent single-phase coolant flowing in line through a reactor-type fuel bundle is described for the prediction of the turbulent heat transport characteristics of the fluid and the fuel element pressure drop. A modified two-dimensional form of the Buleev mixing length theory is used to solve the momentum equation for the subchannel average velocity distribution, and for the distribution of the radial and tangential eddy momentum diffusivity. The effect of the anisotropy of the eddy momentum diffusivity in the wall region on the wall shear stress distribution is examined.

National Library of Australia card number and ISBN 0 642 99684 9

The following descriptors have been selected from the INIS Thesaurus to describe the subject content of this report for information retrieval purposes. For further details please refer to IAEA–INIS–12 (INIS: Manual for Indexing) and IAEA–INIS–13 (INIS: Thesaurus) published in Vienna by the International Atomic Energy Agency.

ANISOTROPY; COOLANTS; FLOW MODELS; FRICTION; FUEL RODS; LAMINAR FLOW; NUMERICAL SOLUTION; RADIAL VELOCITY; REACTOR CHANNELS; TRANSPORT THEORY; TURBULENCE; TURBULENT FLOW

CONTENTS

CONTENTS (Continued)

1. INTRODUCTION

The assessment of the thermal response of a canned uranium dioxide fuel pin, cooled by a single-phase turbulent fluid, requires the development and linking of two detailed mathematical models, one for the two-region fuel rod and the other for the turbulent fluid. This report concentrates on the development of a model of the turbulent transport properties for a single-phase coolant flowing in a four-rod reactor-type subchannel.

The eddy diffusivity concept is used to account for the transport of heat, mass and for momentum interchange by fluid turbulence and, in the turbulent core, the eddy momentum diffusivity is several orders or magnitude greater than the analogous fluid kinematic viscosity. The eddy heat diffusivity is similarly greater than the fluid thermal conductivity for coolants with Prandtl numbers of unity or above, and greatly increases the effective fluid thermal conductivity. For liquid metal coolants, the effect is of the same magnitude as the fluid thermal conductivity, and thus is still significant. The turbulent heat and momentum exchange process within the fluid are usually assumed to be related. To determine the effective thermal conductivity of the fluid, it is first necessary to be able to solve for the fluid average velocity distribution, and the apparent or turbulent eddy viscosity distribution created by the fluid turbulence.

The solution of the time-averaged Navier Stokes or momentum equation for the average velocity field of the viscous single-phase fluid requires a general theory linking the turbulent, or Reynolds stresses with the fluid average point velocity. Although such a general theory does not exist, successful empirical mixing length theories developed by Prandtl and Von Karman [Schlicting 1968] have been used to describe the velocity profile in one-dimensional flow past a plane wall, or in a uniform round duct. The mixing length concept used was generalised by Buleev [1963] to a three-dimensional theory, and this model of the turbulent eddy viscosity was applied to a four-rod subchannel.

A subchannel may be defined generally as the simply connected flow region in a cell, bounded by planes containing the centre lines of adjacent cylindrical rods of a finite or infinite, regular or irregular array of parallel rods. The four-rod subchannel used represents an infinite array of square-pitch parallel rods (Figure 1). This array approximates to the fuel element arrangement of pressurised and boiling light water nuclear reactors, in which the core is built up from box section fuel elements with approximately fourteen by fourteen fuel rods in each element.

The prediction of the average velocity field for turbulent in-line flow through rod bundles has been examined by several authors [Deissler & Taylor 1959; Nijsing, Garganti & Eifler 1966; Shlykov & Tsarevski-Dyakin 1966; Hoffman 1970; Dwyer & Berry 1971] using graphical construction techniques [Deissler & Taylor 1959], and by the transformation of the duct into a circle by a system of orthogonal curvilinear coordinates, the reverse transformation being used to obtain the velocity field [Shlykov & Tsarevski-Dyakin 1966]. In another technique, a universal or logarithmic velocity profile is used along the normal to the rod surface, and an experimentally determined expression for the wall shear stress is used to determine the local shear velocity [Dwyer & Berry 1971]. A problem of this method of analysis is that the zero velocity gradient is not given across the line of symmetry of the subchannel.

The Buleev mixing length theory, in common with that of Shlykov & Tsarevski-Dyakin [1966], assumes that the distribution of the turbulent characteristics over the flow cross section is determined by the geometrical form of the cross section. The eddy diffusivity of momentum at each point in the subchannel is a function of the distance of the point from the walls of the duct, and the total gradient of the average velocity around the point. In common with all the above theories, the fluid properties are considered to be constant. This assumption is of considerable importance in simplifying the solution of the combined heat transfer and fluid flow problem in the duct for heat generating rods, as the energy equation is decoupled from the solution of the momentum Equation (3).

No analytical solution of the turbulent momentum equation, using the Buleev theory to predict the eddy diffusivity of momentum, is possible. This is because the eddy diffusivity of momentum is a function of the average velocity solution, and the momentum equation has thus to be solved by some form of numerical iteration process. However, for the associated laminar flow problem, the eddy momentum diffusivity is zero and a single numerical iteration solves the velocity distribution in the duct.

2. TURBULENT FLOW TIME AVERAGE EQUATIONS

2.1 General Equations

The momentum equations for the average velocity component of a turbulent incompressible fluid are:

$$\frac{\partial(\bar{v}_k)}{\partial t} + \sum_{i=1}^{3} \frac{\partial(\bar{v}_i \bar{v}_k)}{\partial x_i} = -\frac{1}{\rho_f} \frac{\partial \bar{P}}{\partial x_k} + \nu \sum_{i=1}^{3} \frac{\partial^2(\bar{v}_k)}{\partial x_i^2} - \sum_{i=1}^{3} \frac{\partial(\overline{v_i' v_k'})}{\partial x_i} \quad \ldots(1)$$

The equation of conservation of mass is:

$$\sum_{i=1}^{3} \frac{\partial(\bar{v}_i)}{\partial x_i} = 0 \qquad \ldots(2)$$

and the energy equation is

$$\frac{\partial \bar{T}_f}{\partial t} + \sum_{i=1}^{3} \frac{\partial(\bar{v}_i \bar{T}_f)}{\partial x_i} = \alpha \sum_{i=1}^{3} \frac{\partial^2(\bar{T}_f)}{\partial x_i^2} - \sum_{i=1}^{3} \frac{\partial(\overline{v_i' T_f'})}{\partial x_i} \quad . \qquad \ldots(3)$$

The fluid material properties ν, ρ_f and k_f the thermal conductivity are all assumed to be constant.

In Equation (1), the additional terms to the laminar flow form of the Navier Stokes, or momentum equation is the quantity

$$- \rho_f \sum_{i=1}^{3} \frac{\partial(\overline{v_i' v_k'})}{\partial x_i} \quad .$$

This factor represents the additional shearing stresses or Reynolds stresses generated by the turbulent interchange process within the fluid, and no general theoretical method of linking these stresses with the average velocity field has yet been found. However, for single dimension turbulent flow problems in round tubes or past a plane wall, the apparent or turbulent eddy viscosity represented by this term is related by Prandtl to the gradient of the average velocity by an empirical mixing length.

2.2 Fully Developed Turbulent Flow Equations

For asymptotic turbulent in-line flow through a duct of constant cross section, the momentum and energy equations reduce to:

$$\frac{1}{\rho_f} \frac{\partial \bar{P}}{\partial z} = \frac{\partial}{\partial x} \left[(\varepsilon_m^x + \nu)\right] \frac{\partial \bar{V}}{\partial x} + \frac{\partial}{\partial y} \left[(\varepsilon_m^y + \nu)\right] \frac{\partial \bar{V}}{\partial y} \qquad \ldots(4)$$

$$\bar{V}_a \frac{\partial \bar{T}_f}{\partial z} = \frac{\partial}{\partial x} \left[(\varepsilon_h^x + \alpha)\right] \frac{\partial \bar{T}_f}{\partial x} + \frac{\partial}{\partial y} \left[(\varepsilon_h^x + \alpha)\right] \frac{\partial \bar{T}_f}{\partial y} \quad . \qquad \ldots(5)$$

The similarity of the above pair of equations, which govern the heat and momentum transfer process for turbulent asymptotic flow in ducts, forms the basis for analogies between the eddy heat and momentum diffusivities. In the Buleev theory, the eddy momentum diffusivities (ε_m^x and ε_m^y) are functions of the velocity solution, and an iterative numerical method must be used to solve the nonlinear momentum equation. The eddy diffusivities of heat (ε_h^x and ε_h^y) are not, however, functions of the average temperature solution for the fluid, and the energy equation is linear.

3. BULEEV MIXING LENGTH THEORY

3.1 Eddy Diffusivity

There are several features of the three-dimensional mixing length theory, based on Prandtl mixing length concepts, which remove some limitations of earlier mixing length theories. The detailed theory is described extensively by Buleev [1963] and will not be reiterated in depth. The Buleev theory uses a line integral expression for the eddy diffusivity of momentum or heat at each point in the fluid, involving a length scale and the total velocity gradient along the line of integration. This expression applies to all flow regions and does generate zero eddy diffusivity values in the wall region ($y^+ \leqslant 5$).

The use of a line integral, evaluated along the axial direction of the particular eddy diffusivity component, avoids a zero value of diffusivity at points in the fluid where the total velocity gradient is zero.

In addition, this expression allows the different axial components of eddy diffusivity to be of different magnitude, and some allowance is therefore made for the local anisotropy of turbulence in regions where the average velocity gradient is changing rapidly.

3.2 Scale of Turbulence Length

A generalisation of the one-dimensional mixing length or scale of turbulence length is used in the Buleev theory, in which the perpendicular wall distance is replaced by a length proportional to the distance from the point in the fluid to all surrounding walls. This scale of turbulence length is defined by:

$$\frac{1}{L} = \frac{1}{\pi} \int_{4\pi} \frac{1}{\ell(\omega)} \, d\omega \quad . \qquad \ldots(6)$$

For asymptotic flow problems in long straight ducts of constant cross section, this integral can be simplified to:

$$\frac{1}{L} = \frac{1}{2} \int_{2\pi} \frac{1}{\ell(\theta)} \, d\theta \quad . \qquad \ldots(7)$$

For flow past a plane wall, integrals (6) and (7) reduce to the perpendicular wall distance.

The calculation of integral (7) is required at each mesh point for the numerical solution of the momentum equation. The cylindrical system of coordinates was used for the four-rod subchannel, with a point on the centre line of one of the four rods determining the origin.

To evaluate Equation (7) at each point in the mesh, a system of numerical integration was used to find the contribution of each of the four surrounding rods. The angle subtended between a line joining the rod centre and the point in the fluid and one tangential to the rod surface from the same point, is given by:

$$\theta_k = \sin^{-1}\left(\frac{R}{d_k}\right) \quad , \qquad \ldots(8)$$

where k has the values 1 to 4 (Figure 2).

Integral (7) was evaluated for each of the four rods by Gaussian numerical integration [Abramowitz & Stegun 1956], using a three-point approximation.

$$\int_{-\theta_k}^{\theta_k} \frac{1}{\ell(\theta)}\, d\theta = \theta_k \sum_{i=1}^{3} \omega_i f(\theta_i) \quad . \qquad \ldots(9)$$

In Equation (9), ω_i is the weight value, and θ_i is equal to $\theta_k\, x_i$, x_i being the corresponding independent variable interval for the Gaussian integration. The value of $f(\theta_i)$ or $\frac{1}{\ell}(\theta_i)$ is calculated by application of the cosine rule:

$$\ell(\theta_i) = d_k \cos(\theta_i) - \sqrt{R^2 - d_k^2 \sin^2(\theta_i)} \quad . \qquad \ldots(10)$$

The accuracy of the three-point approximation was checked by using a five-point Gaussian approximation at several wall distances from the rod; the answers gave agreement to four figures for each point selected.

For very small distances from the surface of one rod, the scale of turbulence length approaches the perpendicular distances from the point to the rod surface. This is to be expected as the geometry under these conditions approximates to a point near a plane wall.

3.3 Numerical Solution Technique

The symmetry of the average velocity distribution in the infinite array of square-pitch rods was used to reduce the calculational area to one eighth of the total subchannel area (Figure 1). The solution of Equation (4) using the Buleev theory to predict the eddy momentum diffusivity values, requires a numerical iterative process involving two loops. The inner loop determines the velocity solution for a given set of eddy momentum diffusivity values, and the finite difference approximation to the momentum equation was solved by the extrapolated Liebmann process in this loop [Lee & Stone 1959]. The outer loop recalculates the eddy diffusivity values for each converged velocity solution until these values also converge.

The method of solution used is not unconditionally stable, as a good

estimate of the distribution of the eddy diffusivity values has to be used to start the process. In addition, the eddy diffusivity values are related to the total fluid velocity gradient and, consequently, each velocity distribution has to be found accurately before determining new values of these parameters. The initial values of the velocity gradient at each mesh point were found from the radial derivative of the law of the wall velocity distribution for flat plates:

$$V^+ = 5.75 \log_{10} y^+ + 5.50 \quad . \qquad \ldots(11)$$

In the laminar sublayer

$$V^+ = y^+ \quad , \qquad \ldots(12)$$

the radial velocity gradient is constant. The intersection of these two equations at $y^+ = 11.64$ was used to determine the change from a constant radial velocity gradient to one derived from the law of the wall. This procedure does not allow for the transition flow region, located between y^+ values of 5 to approximately 30, and a discontinuity in the radial velocity gradients occurs at the intersection point. The integral expression for the eddy momentum diffusivity (Appendix A) applies to all three regions of the fluid, and the eddy diffusivity values calculated by this expression decay to zero in the region of the rod wall.

4. ROFLO PROGRAM - AVERAGE VELOCITY SOLUTION

4.1 Finite Difference Calculation Mesh

The average velocity distribution in the subchannel calculational area (Figure 1) was solved by the computer program ROFLO, using a two-loop numerical interative procedure (Section 3.3). The solution of Equation (4) for the average velocity field, using a cylindrical geometry mesh based on the centre of one rod, presents some difficulty in the selection of the radial mesh spacing. If equal radial mesh increments were used, the very high velocity gradients in the laminar sublayer adjacent to the rod surface would require a fine mesh spacing in this region. This mesh, however, cannot be extended over the whole calculation area owing to the large number of velocity points created. A logarithmic radial mesh spacing was used, therefore, for the first N-radial mesh points, ER(I); the spacing of this mesh was determined by the wall friction velocity specified for the problem and the rod-gap distance (Figure 3a):

$$A = \frac{20\,\nu}{(p - d)\,\hat{V}^*} \quad , \qquad \ldots(13)$$

$$ER(I) = \frac{(p - d)}{2.0} \left(1 + \frac{1}{A}\right)^{\left(\frac{I}{N} - 1\right)} + R \quad . \qquad \ldots(14)$$

The calculation area angle, $\frac{\pi}{4}$ radian, was divided into N equal segments by N + 1 angular mesh lines.

The matching of the cylindrical geometry radial mesh to the subchannel centre straight-line boundary was achieved by creating an additional radial mesh circle for the intersection of each of the N angular mesh lines outside the rod-gap line (Figure 3b). This system creates an abrupt change in the radial mesh spacing, particularly in the rod-gap region (Figure 3a). The cell average velocity points were located in the centre of each mesh cell, with the exception of the triangular cells located on the subchannel centre line. Here, the corresponding velocity point was placed on the subchannel centre line. The number of radial mesh lines created by this system is 2N, and these values are stored in the program as a column vector ER(I). The mid-point between each pair of radial mesh lines determines the distance of the velocity points from the origin, EA(I).

4.2 Finite Difference Equation

The momentum Equation (4) for the average velocity field in the subchannel, in cylindrical coordinates is:

$$\frac{1}{r}\frac{\partial}{\partial r}\left(r(\varepsilon_m^r + \nu)\frac{\partial \bar{V}}{\partial r}\right) + \frac{1}{r^2}\frac{\partial}{\partial \theta}\left((\varepsilon_m^\theta + \nu)\frac{\partial \bar{V}}{\partial \theta}\right) = \frac{1}{\rho_f}\frac{\partial \bar{P}}{\partial z} \quad . \qquad \ldots(15)$$

In the asymptotic flow conditions, the axial pressure drop is assumed to be constant across the subchannel cross section. The momentum equation was integrated over a mesh cell, bounded by the radial limits r_1 and r_2 and and angular limits θ_1 to θ_2. This cell-integrated form of the finite difference equation was used to minimise the effect of the non-uniform radial mesh spacing, particularly in the subchannel-gap region at the centre line. Integrating Equation (15) between the mesh cell boundaries leads to the equation used to develop the finite difference approximation:

$$\frac{1}{(r_2 - r_1)}\left[\frac{2r_2\ (\varepsilon_m^r + \nu)}{(r_2 + r_1)}\frac{\partial \bar{V}}{\partial r}\bigg|_{r_2} - \frac{2r_1\ (\varepsilon_m^r + \nu)}{(r_2 + r_1)}\frac{\partial \bar{V}}{\partial r}\bigg|_{r_1}\right]$$

$$+ \frac{1}{(\theta_2 - \theta_1)}\ \frac{2}{(r_1 + r_2)}\left[\frac{(\varepsilon_m^\theta + \nu)}{(r_1 + r_2)}\frac{\partial \bar{V}}{\partial \theta}\bigg|_{\theta_2} - \frac{(\varepsilon_m^\theta + \nu)}{(r_1 + r_2)}\frac{\partial \bar{V}}{\partial \theta}\bigg|_{\theta_1}\right] = \frac{1}{\rho_f}\frac{\partial \bar{P}}{\partial z} \quad .$$

$$\ldots(16)$$

The radial and angular eddy diffusivity of momentum values are required by this equation on the four boundaries of the mesh cell (Figure 4), and the radial and angular velocity gradients have also to be evaluated at these boundaries. The radial eddy diffusivity points are located on the same angular lines as the velocity points, but spaced at radial mesh distances from the origin, and the angular eddy diffusivity points are the same distance from the origin as the velocity points, but on the cell mesh angular lines. In the radial velocity gradient term of the cell integrated equation, factor $\frac{2}{r_1 + r_2}$ is EA(I), the distance of velocity point VEL(I,J) from the origin. (See Appendix A for program symbols.)

The solution to the finite difference equation, generated from Equation (16) for the average velocity distribution, was by the Leibmann process [Clark & Hansen 1964]. The value of the extrapolation parameter Ω for this process cannot be estimated by theoretical means, and a satisfactory value of this parameter was determined by a trial substitution of values, and note was taken of the convergence rate.

4.3 Boundary Conditions

In the interative solution of the velocity distribution, a fixed velocity value at some point in the mesh is required to normalise the level of the solution after each iteration. This point was initially selected to be the first velocity point in the rod-gap region, VEL(1,1), and relates to a fixed value of the local wall shear stress. However, subsequent experience in applying the same logarithmic numerical mesh to the solution of the associated laminar flow problem (Section 5) showed that as this region of the velocity field changed the most from the initial velocity distribution, particularly at low rod pitch to diameter (p/d) ratios, fixing a velocity value here caused the program to converge on incorrect solutions. Accordingly, the normalisation point was changed to VEL(1,N) implying a fixed value of the wall shear stress along the radial mesh to the subchannel centre. The three boundaries of the calculation mesh not adjacent to a rod wall form reflection boundaries to the velocity solution, with a zero velocity gradient across them, and the velocity of the fluid at the rod surface is zero. These conditions are used to reduce the normal five-point difference approximation to a three-point approximation at the subchannel centre line, and a four-point approximation at the two angular boundary lines.

5. LAMINAR FLOW PROBLEM

The finite difference equation approximation to the momentum equation, and the associated numerical mesh, was used to solve the laminar flow form

of the momentum equation by equating the ε_m terms to zero:

$$\frac{\nu}{r}\frac{\partial}{\partial r}\left(r\frac{\partial V}{\partial r}\right) + \frac{\nu}{r^2}\frac{\partial^2 V}{\partial \theta^2} = \frac{1}{\rho_f}\frac{\partial p}{\partial z} \quad . \qquad \ldots(17)$$

This was carried out initially as a means of testing the stability and accuracy of the numerical mesh, since the logarithmically spaced radial mesh coupled with the matching of the cells to the subchannel centre line creates very substantial changes in the radial mesh spacing (Figure 3a). It was found that the location of the single fixed velocity value, used to normalise the velocity distribution after each numerical iteration, did influence the stability of the numerical solution for laminar flow. However, when located in a part of the velocity field away from the rod-gap area, the process was stable and converged to a unique solution.

The solution of the laminar flow momentum equation also provides a means of estimating the error in the infinite rod array velocity distribution created by placing a wall across the rod gap. This problem has some practical importance, as flow in rod subchannels is experimentally studied by using two interconnected subchannels as a test duct with all other rod gaps blanked off (Figure 5a).

In the numerical solution of the closed rod-gap problem (Figure 5b), the zero velocity condition at this wall can conveniently be generated by using a negative mirror image velocity equidisdant from, and on the other side of the gap wall to the first radial velocity line. For laminar flow conditions, the momentum equation can be solved analytically for approximately the same geometry, using bipolar coordinates (Appendix B). An analytic estimate of the accuracy of the numerical solution can thus be made.

In turbulent flow conditions, the error involved in using the closed duct (Figure 5a) to represent an infinite square-pitch rod array in the rod-gap area shown would be considerably less. This is because the velocity gradient adjacent to the duct walls is far greater than for laminar flow, and the effect of the wall in the rod gap would consequently have less influence on the subchannel velocity distribution.

The error in the numerically calculated velocity distribution along the subchannel centre line, from the infinite rod array solution to the closed duct solution (Figure 5b), is shown by Figure 6. The approximate analytic solution, using only the first term of the series expansion, is also shown; for low (p/d) ratios ($p/d \leqslant 1.10$) the agreement is good. The distortion introduced into the velocity distribution by the rod-gap wall is seen to be strongly dependent on the (p/d) ratio. For widely spaced rods ($p/d = 1.50$),

the magnitude of the error at the subchannel centre is estimated to be 1.1 per cent, which is considerably less than the 5 per cent predicted by the analytic solution. This discrepancy is due partly to the inaccuracy of the theoretical model in the subchannel centre, and partly because only the first term of the series expansion was used to determine the velocity distribution along the subchannel centre line.

6. RESULTS

6.1 General

A parametric study was made to determine the subchannel velocity, eddy momentum diffusivity, and subchannel friction factor as a function of the rod pitch to diameter (p/d) ratio and the flow Reynolds number (Re). The rod diameter was held constant at 15.24 mm (0.60 inch) and the fluid properties used represented saturated water at 280°C. The (p/d) ratio was varied between 1.04 and 1.80, though more detailed attention was given to the lower (p/d) ratios (1.04 and 1.10), as these show the largest variation in the rod wall shear stress distribution and the subchannel eddy momentum diffusivity distribution.

6.2 Friction Factor

The subchannel friction factor (fs) compared to the round tube friction factor (f) is shown as a function of the (p/d) ratio by Figure 7, for a Reynolds number of 5×10^4. The Blasius expression, applicable for Reynolds numbers below 10^5, was used to calculate the round duct friction factor (f)

$$f = 0.3164\ Re^{-0.25} \quad . \qquad \ldots(18)$$

In common with the theoretical predictions of Ramm & Johannsen [1971], the subchannel friction factor is below the round tube friction factor for (p/d) values less than 1.10. However, for a (p/d) ratio of 1.80 the predicted friction factor ratio (fs/f) is above the ratio predicted by these authors by approximately 15 per cent. Experimental results for single-phase flow in four-rod subchannels show considerable scatter [Green & Hooper 1973; Marek, Maubach & Rehure 1973] and, although experimental friction factors are above the round tube values for (p/d) ratios greater than 1.1, there is not sufficient accuracy to substantiate either of the theoretical predictions at the larger (p/d) ratios.

6.3 Wall Friction Velocity and Shear Stress Distribution

The maximum wall friction velocity ($\hat{V}^*$) and the maximum wall shear stress ($\hat{\tau_w}$) occur at the point on the rod wall cut by the subchannel diagonal, and the minimum of both these variables in the rod gap. These results are

consistent with experimental results for developed turbulent flow in symmetrical three-rod subchannels [Subbotin *et al.* 1971].

The maximum rod wall friction velocity is specified as part of the input data in the ROFLO program, and this value is directly related to the subchannel Reynolds number (Figure 8). This relationship can be generalised to other fluid properties and rod dimensions by using the average wall friction velocity Reynolds number, $\bar{V}^* d_H/\nu$, based on the average wall friction velocity, $\bar{V}^*$ (Figure 9).

The wall shear stress variation is a function of both the rod spacing or (p/d) ratio, and the flow Reynolds number. The magnitude of the variation in the rod wall shear stress, $\tau_w(\theta)$, and wall friction velocity, $V^*(\theta)$, is strongly dependent on the rod spacing or (p/d) ratio, the maximum variation occurring at a (p/d) ratio of 1.0. This configuration, in which the rods are touching, could not be calculated by the ROFLO program without substantial modification to the numerical mesh. However, the program operates at a (p/d) ratio of 1.04, and this rod spacing closely approximates the limiting case.

The variation of the wall shear stress around the rod is also a function of the flow Reynolds number, and the magnitude of the variation decreases with increasing Reynolds number. This is to be expected, as the thickness of the laminar sublayer decreases with increasing Reynolds number, and the intensive momentum exchange process in the turbulent core region of flow acts to equalise the rod wall shear stress distribution. The predominant factor influencing the variation of wall shear stress is, however, the (p/d) ratio of the rod array (Figure 10).

6.4 Velocity Distribution

The radial velocity profiles at several values of θ from the rod gap ($\theta = 0$) to the radial line joining the subchannel centre ($\theta = \pi/4$) are shown by Figure 11, for (p/d) ratios of 1.04 and 1.10. For comparison, the law of the wall velocity based on the corresponding wall friction velocity is shown, and for both (p/d) ratios the maximum error between the velocity profiles near the rod surface occurs in the rod-gap area. The law of the wall velocity profile fits the predicted velocity distribution along the subchannel diagonal ($\theta = \pi/4$) more accurately for the (p/d) ratio of 1.10, although the fit in the wall region is more accurate at the lower (p/d) ratio.

A point plot of the velocity values, interpolated at equal velocity increments from the velocity distribution, is shown by Figure 12, together with the 30-point angular mesh used. A smooth curve fit to the same isotachs is shown for the whole subchannel area by Figure 13, and this shows the

compression of the contours towards the rod surface in the subchannel centre region, where the wall shear stress is also at a maximum.

6.5 Eddy Momentum Diffusivity

The ratio of the radial eddy diffusivity of momentum to the fluid kinematic viscosity (ε_m^r/ν), from the rod gap ($\theta = 0$) to the subchannel diagonal ($\theta = \pi/4$), shows the radial momentum diffusivity distribution to be similar to curves for round ducts [Quarmby & Quirk 1972], particularly for the profile along the subchannel diagonal (Figures 14a, b). The Prandtl mixing length theory predicts a parabolic distribution of ε_m^r for turbulent flow in round ducts, with the maximum value of ε_m^r given by the dimensionless ratio ($\hat{\varepsilon}_m^r/RV^*$) being equal to 0.10, where V^* is the wall friction velocity and R the duct radius [Hooper 1963]. The eddy diffusivity falls to zero at the wall and the pipe centre line. This zero value at the centre line shows one limitation of the mixing length approach, as the turbulent diffusion process does not necessarily become zero at points of constant average velocity. By integrating a function of the velocity gradient along the supposed path length of the eddy to determine ε_m^r, the Buleev theory avoids a zero value at points of no average velocity gradient.

There is little experimental information of the eddy momentum diffusivity distribution in rod subchannels, and the predicted maximum values ($\hat{\varepsilon}_m^r$) for this geometry were compared with the Prandtl theory for fully developed flow in round ducts (Figure 15). Experimental results of measurements of the analogous eddy mass diffusivity for flow in round ducts have also been made, using a tracer fluid injected into the duct centre and determining the average concentration profiles at axial stations downstream. The method of analysis generally used permits only the average value of the eddy mass diffusivity to be found for the centre region of the duct.

In contrast to the Prandtl theory, the eddy diffusivity is assumed to be constant. The eddy mass diffusivity values determined by Towle & Sherwood [1939] and later by Sheriff & O'Kane [1971] were also compared with the predicted momentum diffusivities for the subchannel geometry (Figure 15), and both the momentum and mass values show a different gradient to the subchannel values when plotted against the Reynolds number.

Mixing experiments have been conducted for flow in four-rod subchannels [Van der Ros & Bogaardt 1970; Green & Hooper 1973], using a similar method to that of Towle & Sherwood to determine the average eddy mass or heat diffusivity in the subchannel centre region. The experimental values of the average eddy diffusivities show a similar relation to the rod spacing and

subchannel Reynolds number and, assuming that the turbulent Prandtl or Schmidt number is approximately unity, support the numerical prediction that the subchannel centre eddy diffusivity is directly proportional to the Reynolds number:

$$(\hat{\varepsilon}_m^r/\nu) = C \; Re \; . \qquad \ldots(19)$$

The value of the constant C is a function of the rod spacing or (p/d) ratio, and applies for flow in rod bundles without grids or spaces. The work of Van der Ros & Bogaardt [1970] shows a considerably higher value of this constant than predicted for the (p/d) ratio of 1.33, and this is probably due to the presence of grids in their four-rod subchannels. Other work quoted by them shows good agreement with the predicted curves (Figure 15).

The Buleev theory is perhaps unique in that a separate expression to the radial component is used to predict the angular or tangential eddy momentum diffusivity [Quarmby & Quirk 1972, 1974]. However, although an approximation to the theory was used to evaluate the tangential component, by integrating along a constant radius mesh instead of the tangent to this mesh, this approximation is most accurate in the wall region where the short arc length of integration closely approximates the tangent. It is in the wall region that recent experimental work [Quarmby & Quirk 1972, 1974] has shown that the ratio between the tangential and radial eddy diffusivities may approach as much as 100 before the laminar sublayer is entered, though the ratio is unity over most of the turbulent core. The ratio between the tangential and radial momentum diffusivities as predicted by the Buleev theory is substantially unity over the whole subchannel. This theory does not predict the anisotropy of turbulence in the wall region, and this defect has also been noted by Ramm & Johannsen [1972], who have proposed a modification to the theory to account for this effect.

The anisotropy of turbulence near a duct wall is probably caused by the greater attenuation of the radial diffusivity component normal to the wall surface than the tangential eddy diffusivity; this effect has considerable influence on the variation of the wall shear stress distribution, and on the related surface heat transfer coefficient.

6.6 Representation of Wall Turbulence Anisotropy

The effect of the anisotropy of the wall turbulence on the subchannel velocity distribution, wall shear stress distribution and friction factor was tested by multiplying the tangential component of the eddy momentum diffusivity by a weighting function, chosen to fit approximately the

experimental results of Quarmby & Quirk [1972] for round tubes:

$$W_f = 50 \exp(-40y/(\sqrt{2}\ p - d)) + 1.0 \quad . \qquad \ldots(20)$$

The weighting function (W_f) has a value of nearly unity over most of the subchannel and becomes of significant magnitude only in the rod wall region.

Two values of rod spacing were used to assess the effect of this weighting function, with (p/d) ratios of 1.04 and 1.10. The effect of the weighting function on the subchannel velocity distribution was to slightly decrease the ratio of the peak velocity to the subchannel average velocity. The radial velocity profiles based on the law of the wall (Appendix A) were brought into closer agreement with the predicted profiles, and the subchannel friction factors increased by 8 per cent for the (p/d) ratio of 1.04, and by 4.5 per cent for the (p/d) ratio of 1.10. Both of these effects may be related to the variation in the wall shear stress distribution, as the effect of the anisotropy of wall turbulence decreases the magnitude of the change in the wall shear stress in the rod gap by 24 per cent for a (p/d) ratio of 1.04, and by 18 per cent for the 1.10 ratio (Figure 16).

The wall shear stress distribution is, therefore, the parameter most sensitive to the anisotropy of turbulence near the rod surface, which acts to equalise the surface shear stress. Although the wall shear stress variation is smaller for reactor rod bundle spacings (p/d from 1.20 to 1.50), the anisotropy of wall turbulence also acts to limit the rod surface temperature variation due to non-uniform surface heat fluxes, and is important in the related heat transfer problem.

7. CONCLUSIONS

- The radial velocity profiles predicted show fair agreement with the law of the wall expression, based on the local value of the wall friction velocity.
- The relationship between the rod spacing, maximum eddy diffusivity and subchannel Reynolds number is predicted to be of the form:

  $$(\hat{\varepsilon}_m/\nu) = C\ Re\ ,$$

  where the constant C is determined by the rod spacing. This expression appears to be consistent with experimental work, and provides a means of estimating the subchannel eddy diffusivity for in-line flow through unbaffled four-rod subchannels. As such, it also provides a means of comparing experimental eddy diffusivities for flow in fuel bundles with grids and spaces, and thus to estimate the effect of such grids on turbulent mixing in the centre of the

subchannel.

- The Buleev theory does not predict the anisotropy of eddy diffusivity in the wall region, and this effect is important in equalising both the wall shear stress distribution and temperature in the related heat transfer problem.
- The variation of the rod wall shear stress is a strong function of the rod spacing, and only slightly depends on the flow Reynolds number. This result is supported by the detailed experimental work of Subbotin *et al.* [1971], for flow in three-rod subchannels.
- For laminar flow in four-rod subchannels, it has been shown that the presence of a wall in the rod gap does not extend far into the velocity distribution, for reactor-type rod spacings ($p/d \leqslant 1.50$). In turbulent flow conditions, and neglecting secondary flow effects, the presence of the wall would have less influence, due to the correspondingly higher velocity gradients near walls. It appears reasonable to study flow in ducts of the cross section of Figure 5a.

8. NOTATION

A_f	subchannel area
R	rod radius
d	rod diameter
p	rod pitch
(p/d)	rod pitch/diameter ratio
d_H	subchannel hydraulic diameter ($4A_f/\pi d$)
ν	fluid kinetic viscosity
ρ_f	fluid density
k_f	fluid thermal conductivity
c_{pf}	fluid specific heat
α	fluid thermal diffusivity ($k_f/\rho_f \nu c_{pf}$)
V	fluid point velocity ($V = V' + \bar{V}$)
$\bar{V}$	average fluid point velocity
V'	turbulent component of fluid point velocity
$\bar{V}_a$	subchannel average velocity
v_i or (u,v,w)	components of V along reference axis
v_i' or (u',v',w')	components of V' along reference axis
$\bar{v}_i$ or $(\bar{u},\bar{v},\bar{w})$	components of $\bar{V}$ along reference axis
$\bar{T}_f$	fluid average point temperature
t	time

Re	Reynolds number for subchannel ($\bar{V}_a d_{HE}/\nu$)
P	fluid pressure
Pr	fluid Prandtl number (ν/α)
ϵ_m	eddy momentum diffusivity } Superscript (x,y) or (r,θ)
ϵ_h	eddy heat diffusivity } refers to axial direction
τ	fluid shear stress
τ_w	fluid shear stress at wall
y	perpendicular wall distance
$\hat{y}$	wall distance to subchannel line of symmetry
V^*	wall friction velocity ($\sqrt{\tau_w/\rho_f}$)
$\hat{V}^*$	maximum wall friction velocity
y^+	dimensionless wall distance (yV^*/ν)
V^+	dimensionless velocity (V/V^*)
$\ell(\theta)$	wall distance at angle θ
d_k	tangent length from subchannel point to rod k(k = 1 - 4)
L	Buleev scale of turbulence length
L_o	scale of turbulence length at reference point
Ω	extrapolation parameter (finite difference equation)

9. ACKNOWLEDGEMENT

The encouragement and assistance of Professor J.J. Thompson in this work is gratefully acknowledged.

10. REFERENCES

Abramowitz, M., & Stegun, I.A. [1965] - Handbook of Mathematical Functions. Dover Publications Inc., New York.

Buleev, N.I. [1963] - Theoretical Model of Mechanism of Turbulent Exchange in Fluid Flows. AERE Trans. 957.

Clark, M. & Hansen, K.F. [1964] - Numerical Methods of Reactor Analysis. Academic Press, New York.

Deissler, R.G. & Taylor, M.F. [1957] - Analysis of Axial Turbulent Flow and Heat Transfer Through Banks of Rods and Tubes. USAEC Report TID 7529 (Pt.1) Book 2, p.416.

Dwyer, O.E. & Berry, H.C. [1971] - Turbulent Flow Heat Transfer for In Line Flow Through Unbaffled Rod Bundles. *Nucl. Sci. Eng.* 46 : 284-303.

Faddeeva, V.N. [1959] - Computational Methods of Linear Algebra. Dover Publications Inc., New York.

Green, W.J., & Hooper, J.D. [1973] - An Experimental Investigation of the Turbulent Exchange of Mass Between Rod Subchannels. First Australas. Conf. on Heat and Mass Transfer, Monash University, Melbourne, Monash University Press. Section 4.2, p.41

Hoffman, F. [1970] - Velocity and Temperature Distribution in Turbulent Flow in Sodium Cooled Fuel Elements with Eccentric Geometry. *Nucl Nucl. Eng. Des.* 14 : 43-50.

Hooper, G.T.J. [1963] - Turbulent Momentum Diffusivity Within a Circular Tube. *Int. J. Heat Mass Transfer.* 6 : 805-812.

Kerstin, J. & Richardson, P.D. [1963] - Heat Transfer Across Turbulent Incompressible Boundary Layers. *Int. J. Heat Mass Transfer.* 6 : 147-189.

Marek, J., Maubach, K., & Rehure, K. [1973] - Heat Transfer and Pressure Drop Performance of Rod Bundles Arranged in Square Arrays. *Int. J. Heat Mass Transfer.* 16 : 2215-2228.

Nijsing, R., Gargantini, I. & Eifler, W. [1966] - Analysis of Fluid Flow and Heat Transfer in a Triangular Array of Parallel Heat Generating Rods. *Nucl. Eng. Des.* 4 : 375-398.

Quarmby, A. & Quirk, R. [1972] - Measurements of the Radial and Tangential Eddy Diffusivities of Heat and Mass in Turbulent Flow in a Plane Tube. *Int. J. Heat Mass Transfer.* 15 : 2309-2327.

Quarmby, A. & Quirk, R. [1974] - Axisymmetric and Non-axisymmetric Turbulent Diffusion in a Plain Circular Tube at High Schmidt Number. *Int. J. Heat Mass Transfer.* 17 : 143-147.

Ralston, A. & Wilf, H. [1960] - Mathematical Methods for Digital Computers. John Wiley & Sons, New York.

Ramm, H., & Johannsen, K. [1971] - Radial and Tangential Turbulent Diffusivities for Heat and Momentum Transfer in Liquid Metals. Conference paper, International Centre for Heat and Mass Transfer - Heat Transfer in Liquid Metals Seminar, September, TROGIR, Yugoslavia.

Ramm, H. & Johannsen, K. [1972] - Hydrodynamics and Heat Transfer in Regular Arrays of Circular Tubes. Conference paper, International Centre for Heat and Mass Transfer - Recent Developments in Heat Exchangers Seminar, August/September, TROGIR, Yugoslavia.

Schlicting, H. [1968] - Boundary Layer Theory. McGraw Hill, New York.

Sheriff, N. & O'Kane, D.J. [1971] - Eddy Diffusivity of Mass Measurements for Air in a Circular Duct. *Int. J. Heat Mass Transfer.* 14 : 697-707.

Shlykov, Yu. P. & Tsarevski-Dyakin, S.N. [1966] - Turbulent Flow and Heat Exchange in Smooth Straight Channels of Any Cross Section. *Therm. Eng.* 13 (12) 62. *(Trans. Teploehnergetika (USSR)).*

Subbotin, V.I., Ushakov, P.A., Leuchenko, Yu. D. & Aleksandrov, A.M. [1971] -

Velocity Fields in Turbulent Flow Past Rod Bundles. *Heat Transfer Sov. Res.* 3 (2) 9-35.

Towle, W.L. & Sherwood, T.K. [1939] - Eddy Diffusion - Mass Transfer in Central Region of a Turbulent Air Stream. *Ind. Eng. Chem.* 31 (April) 457.

Van der Ros, R. & Bogaardt, M. [1970] - Mass and Heat Exchange Between Adjacent Channels in Liquid Cooled Rod Bundles. *Nucl. Eng. Des.* 12 : 259-268.

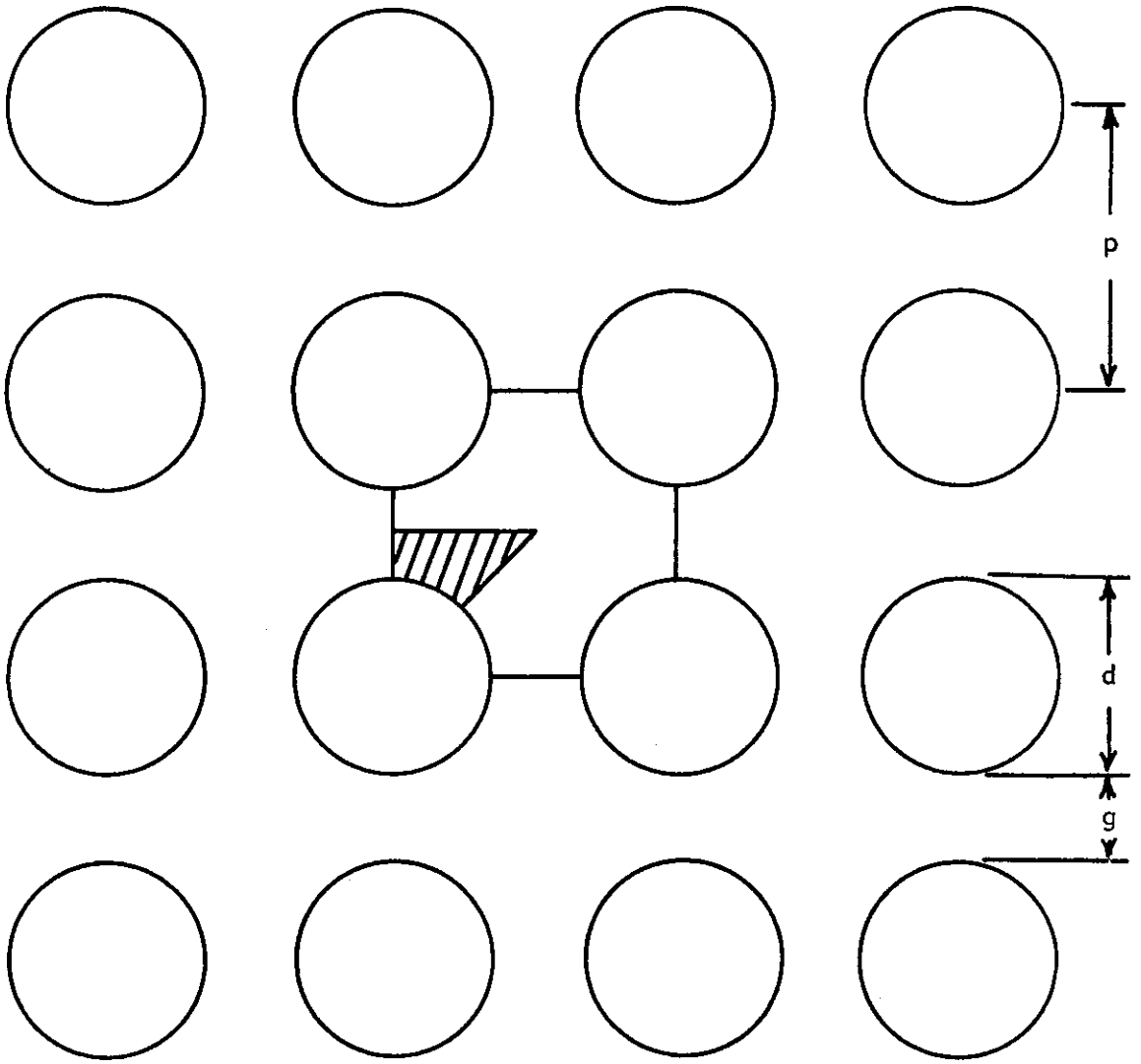

p - rod pitch, g - rod gap, d - rod diameter. Shaded area shows smallest symmetrical component of the subchannel. Pitch to diameter ratio (p/d) = 1.50

FIGURE 1. FOUR-ROD SUBCHANNEL IN A SQUARE PITCH ROD ARRAY

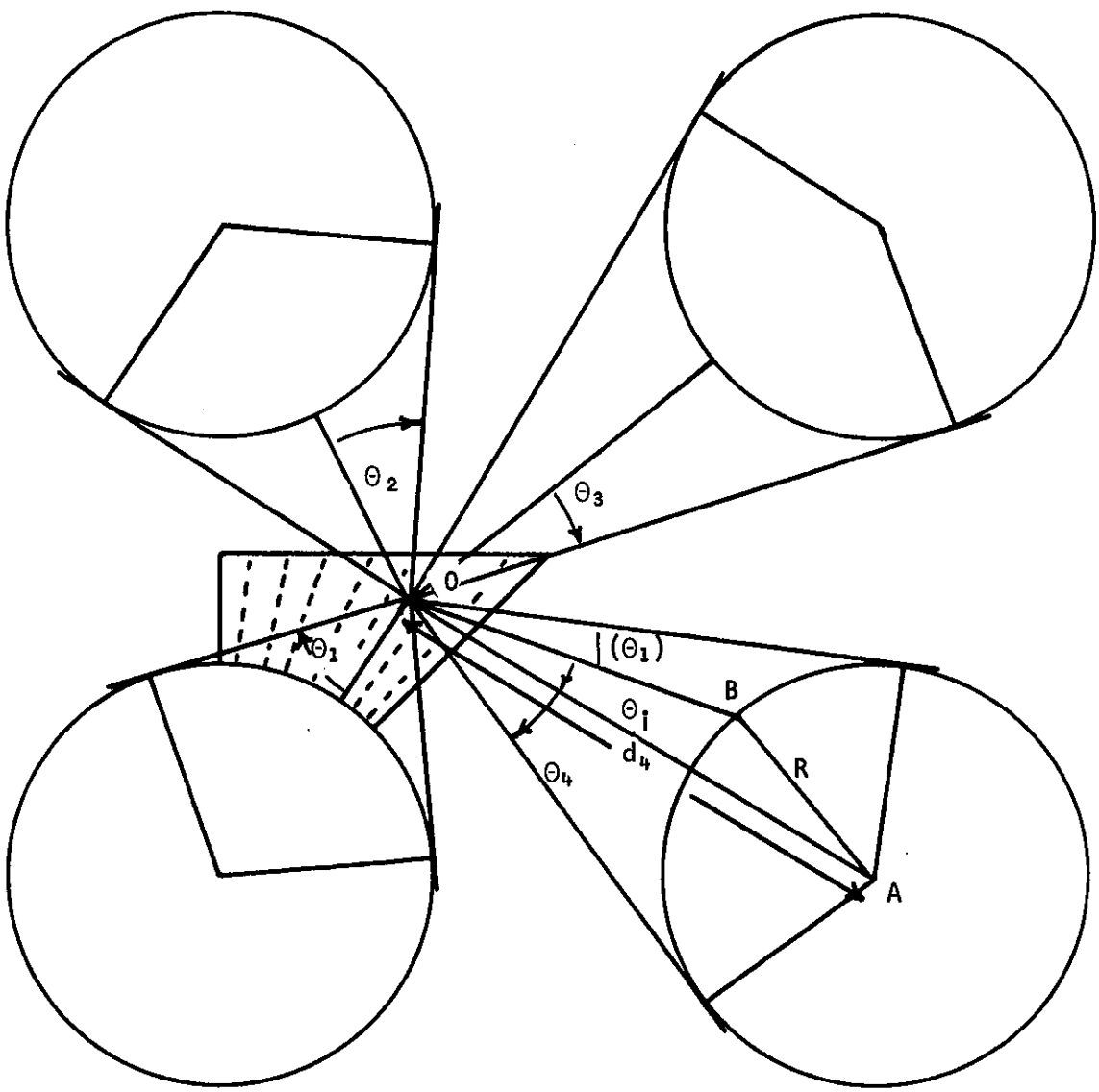

Mesh area shown shaded. Cosine rule applied to triangle OAB:

$$\ell(\Theta_i) = d_4 \cos(\Theta_i) - (R^2 - d_4^2 \sin^2(\Theta_i))^{1/2}$$

FIGURE 2. SCALE OF TURBULENCE CALCULATION FOR POINT O

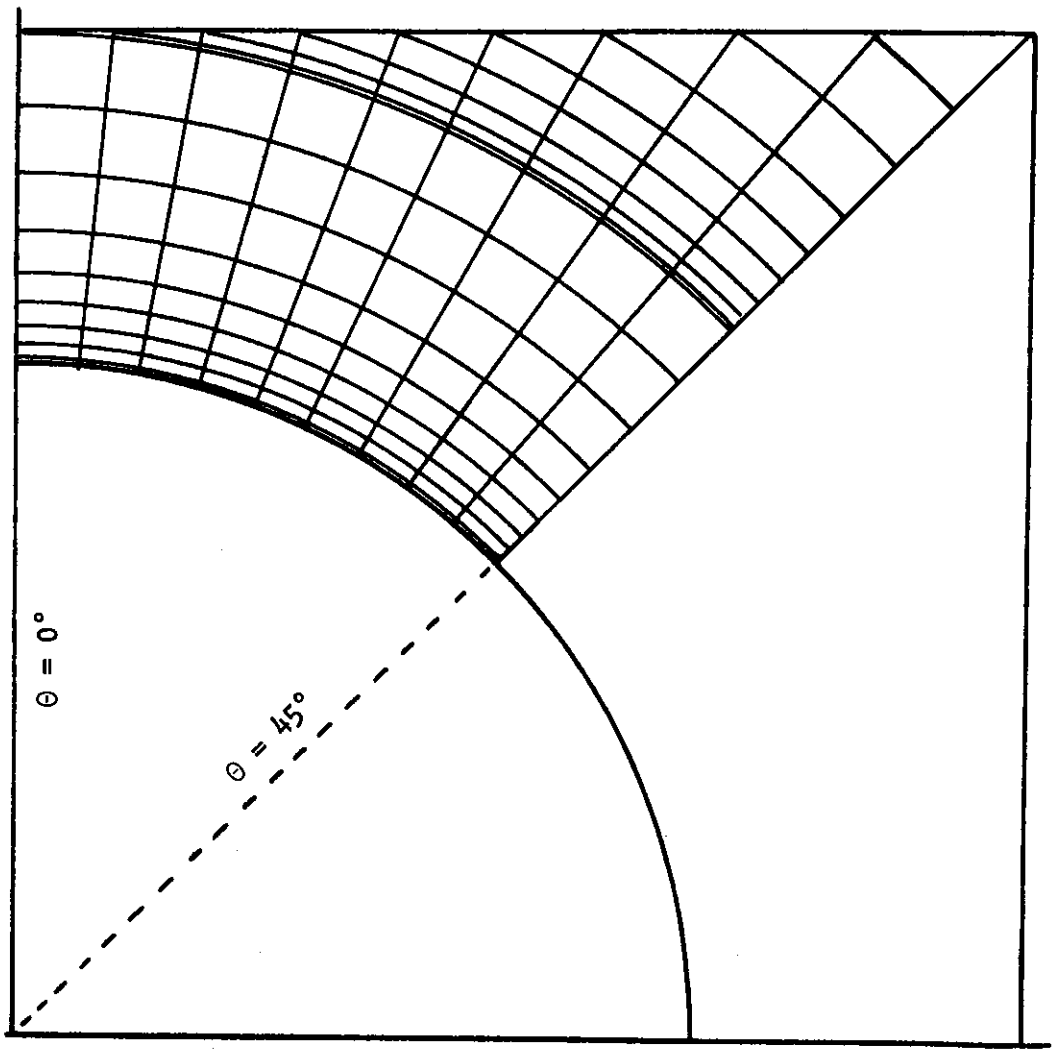

FIGURE 3(a) RADIAL MESH FOR N=9 ANGULAR SEGMENTS

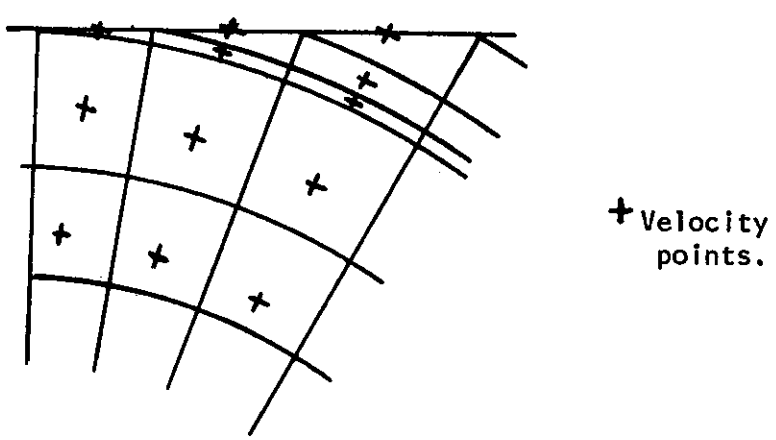

FIGURE 3(b) MATCHING RADIAL MESH POINTS TO THE SUBCHANNEL CENTRE LINE

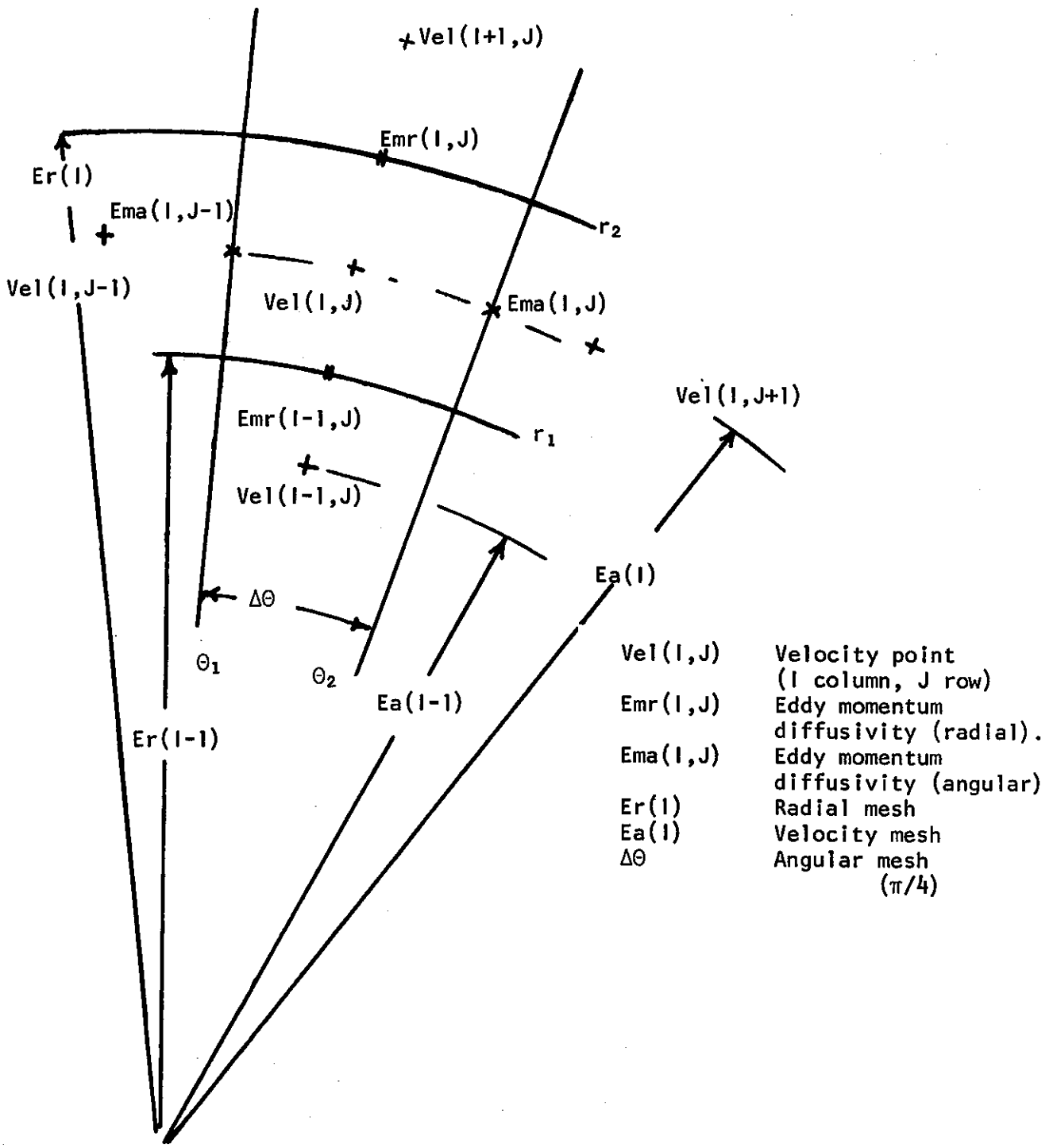

FIGURE 4. CYLINDRICAL CO-ORDINATE MESH CELL

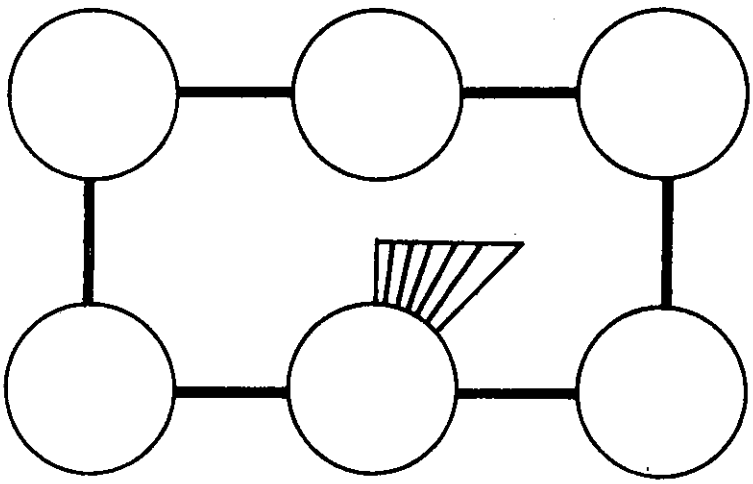

Shaded area closely approximates infinite rod array.

FIGURE 5(a) TWO INTERCONNECTED SUBCHANNELS FORMING EXPERIMENTAL DUCT

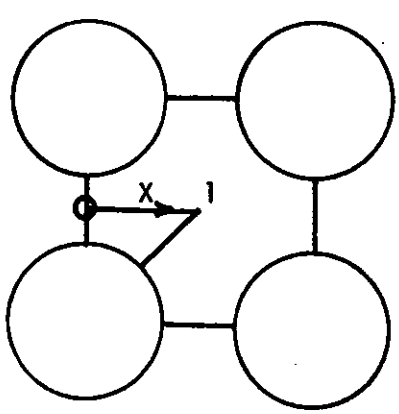

Closed four-rod array.
Velocity solution $V_s(r,\Theta)$.

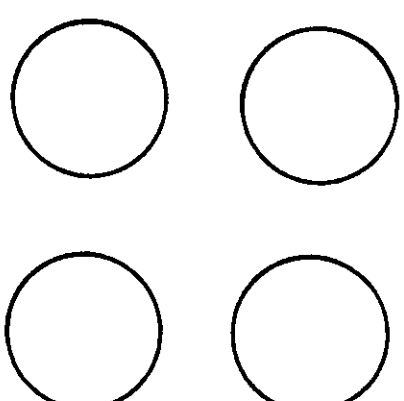

Infinite rod array.
Velocity solution $V_\infty(r,\Theta)$.

FIGURE 5(b) ERROR BETWEEN VELOCITY DISTRIBUTION ALONG THE SUBCHANNEL CENTRE LINE IS $1 - \frac{V_s(r,\theta)}{V_\infty(r,\theta)}$

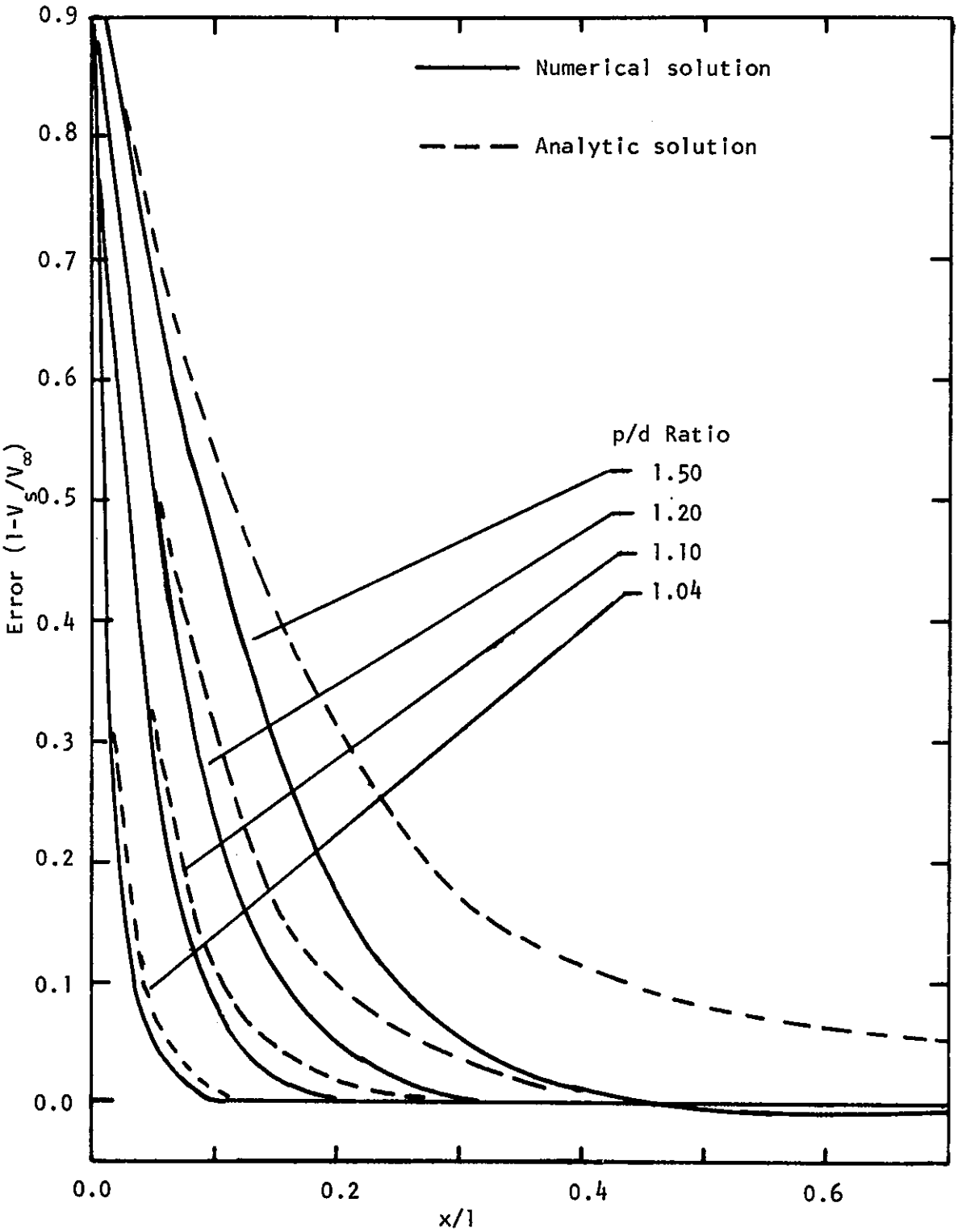

FIGURE 6. ERROR BETWEEN LAMINAR FLOW SOLUTION IN A CLOSED AND INFINITE FOUR-ROD ARRAY

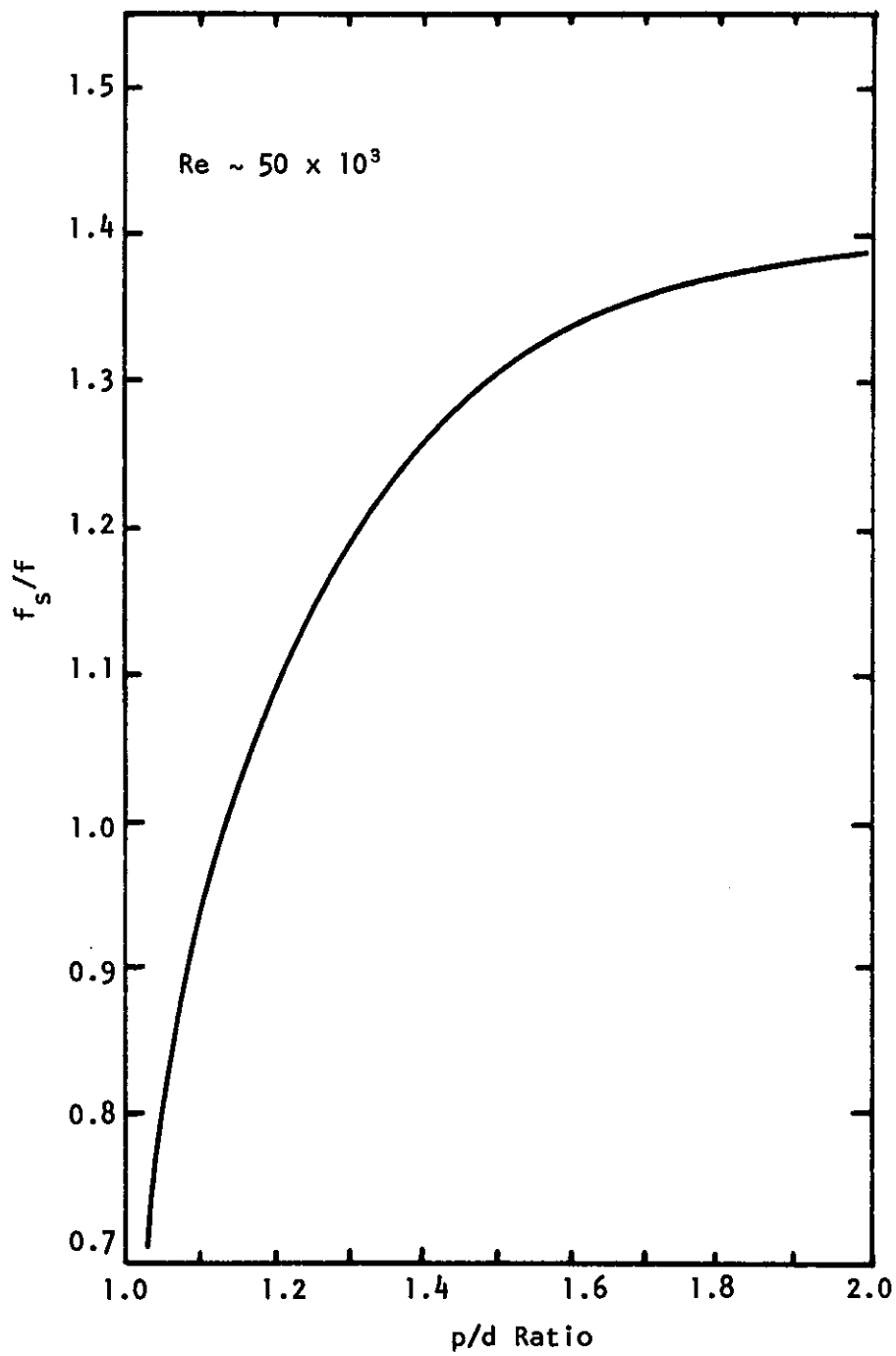

FIGURE 7. SUBCHANNEL FRICTION FACTOR/ROUND DUCT FRICTION FACTOR

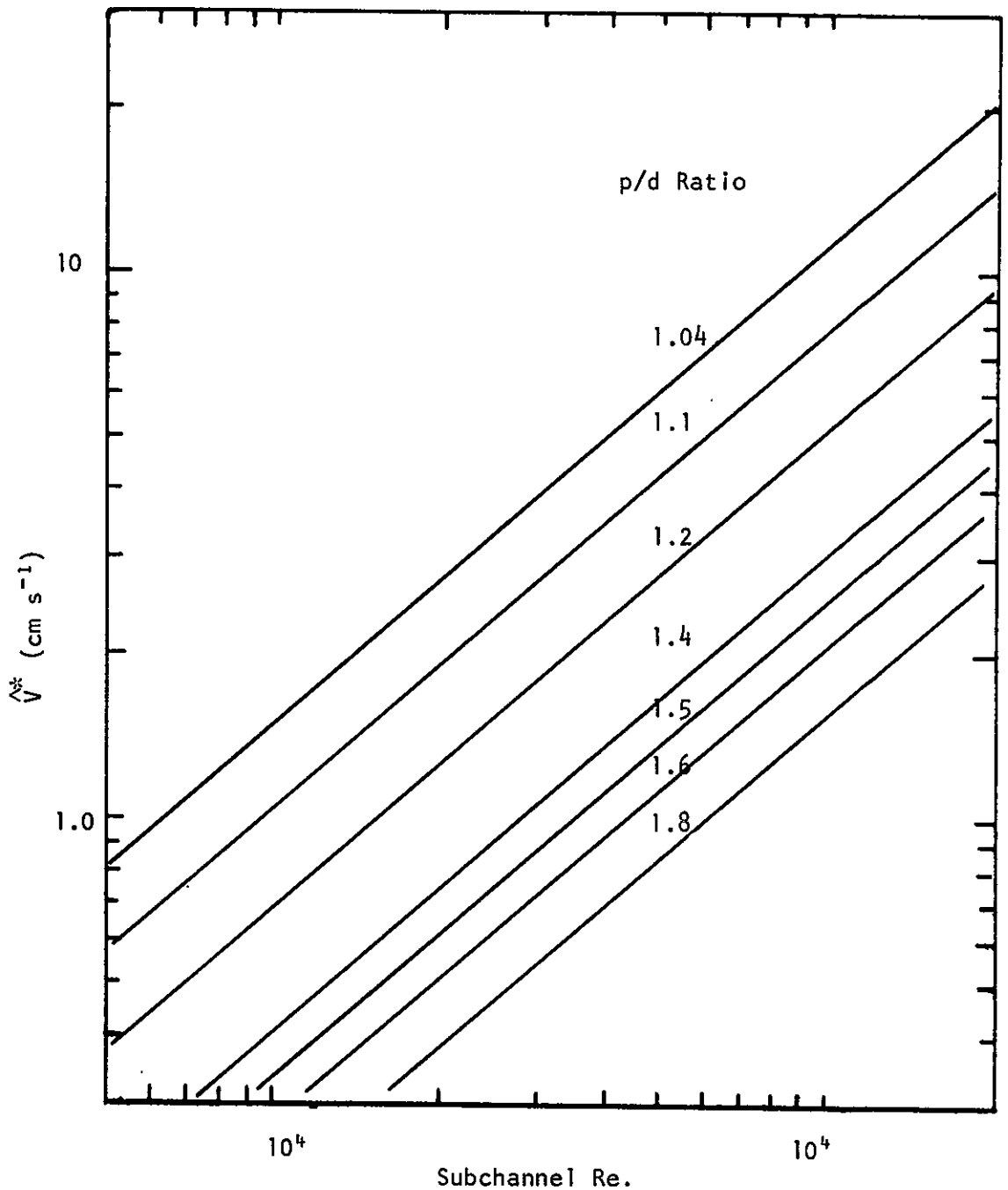

FIGURE 8. MAXIMUM WALL FRICTION VELOCITY ($\hat{V}^*$) AS A FUNCTION OF THE SUBCHANNEL REYNOLDS NUMBER

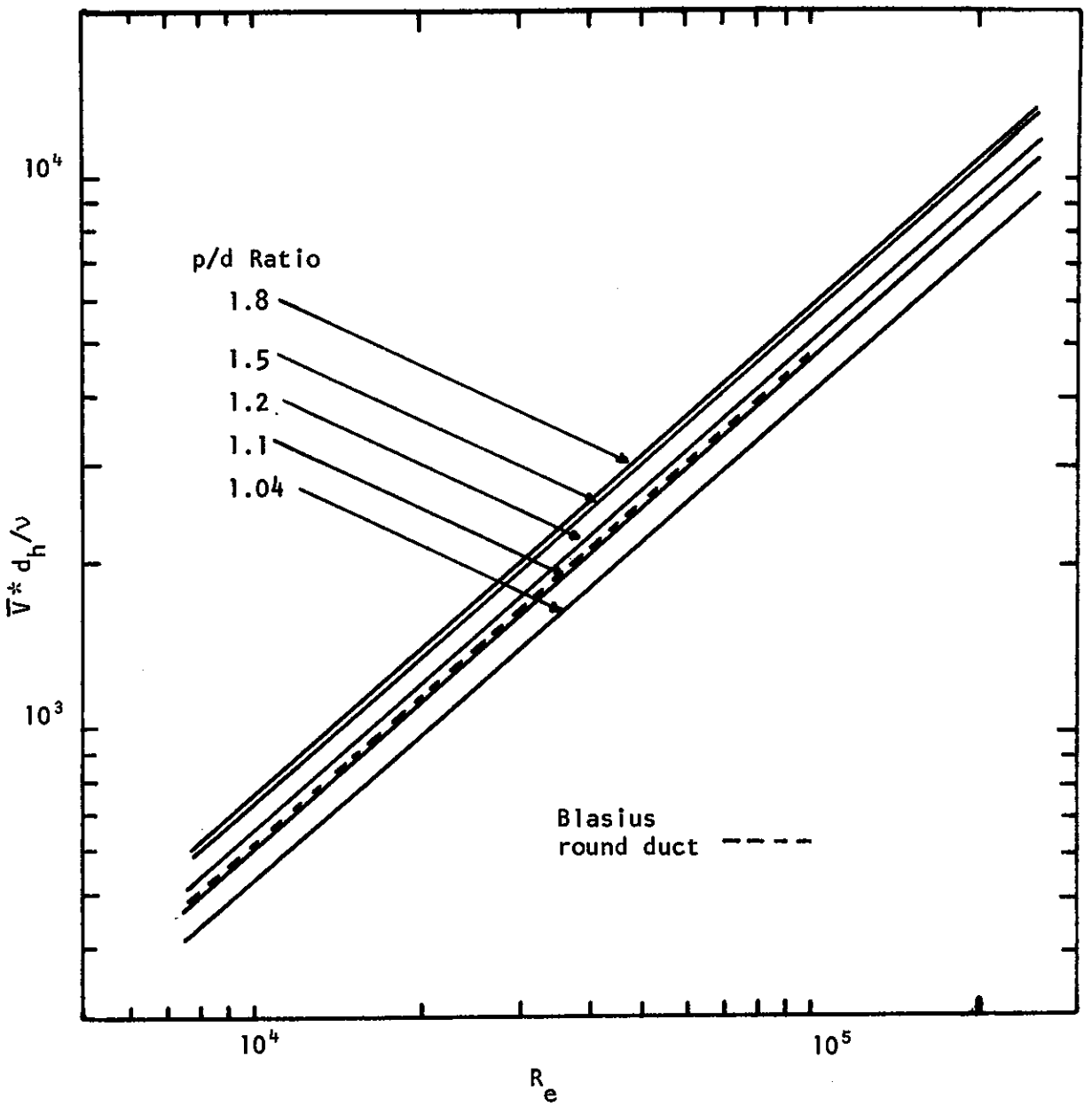

FIGURE 9. AVERAGE WALL FRICTION VELOCITY REYNOLDS NUMBER ($\bar{V}^* d_h/\nu$) AS A FUNCTION OF THE SUBCHANNEL REYNOLDS NUMBER

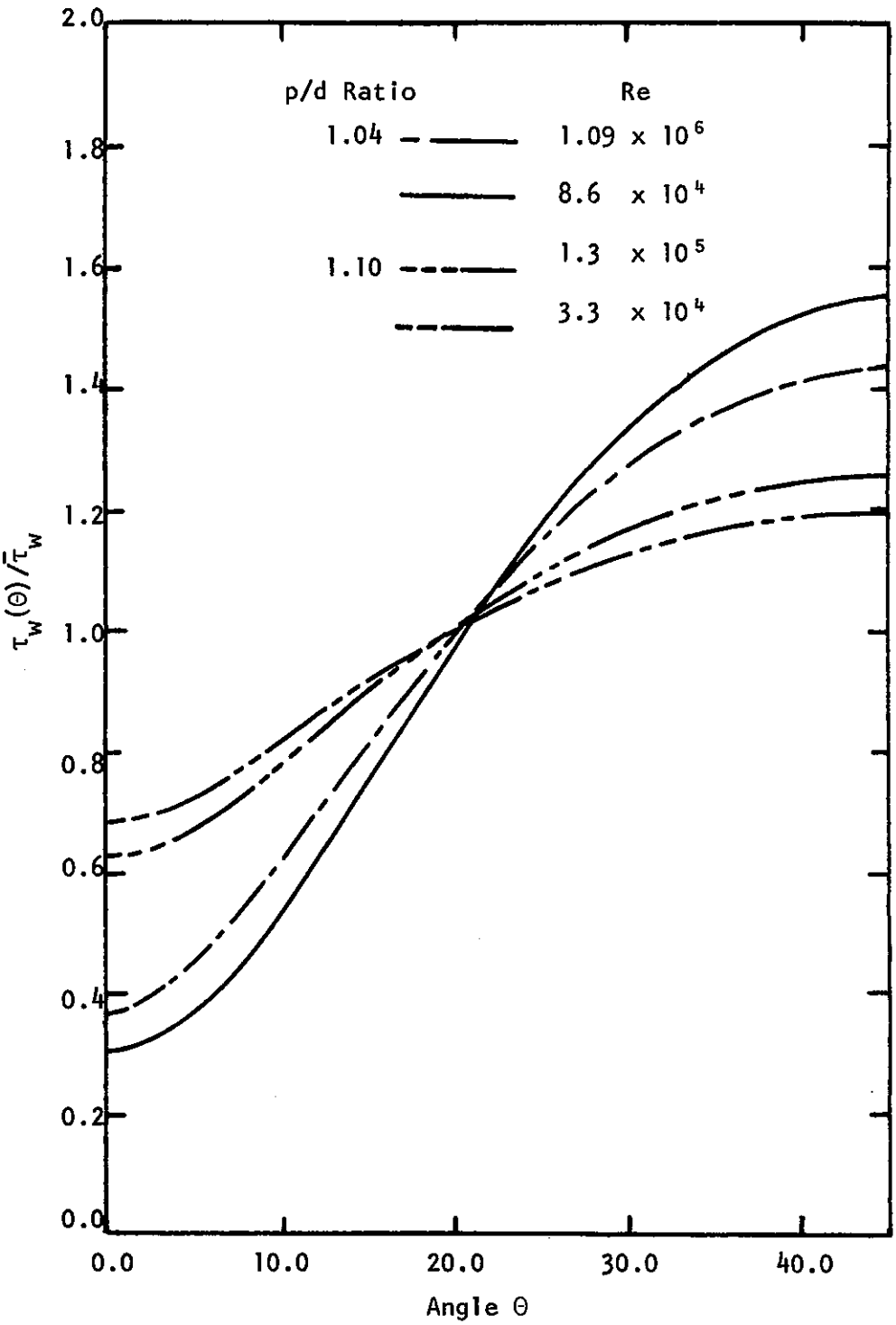

FIGURE 10. WALL SHEAR STRESS ($\tau_w(\theta)$)

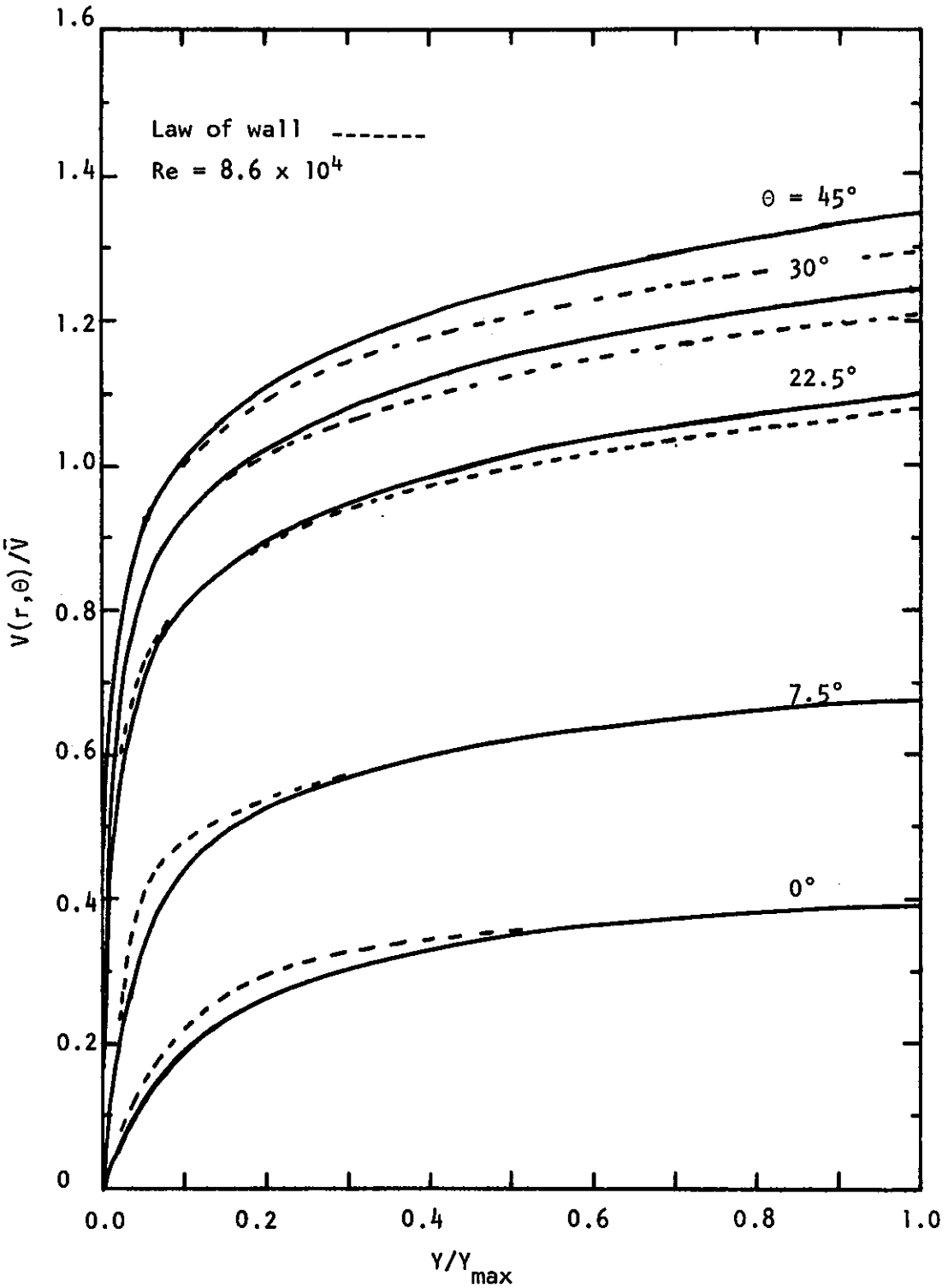

FIGURE 11(a) RADIAL VELOCITY PROFILE (p/d = 1.04)

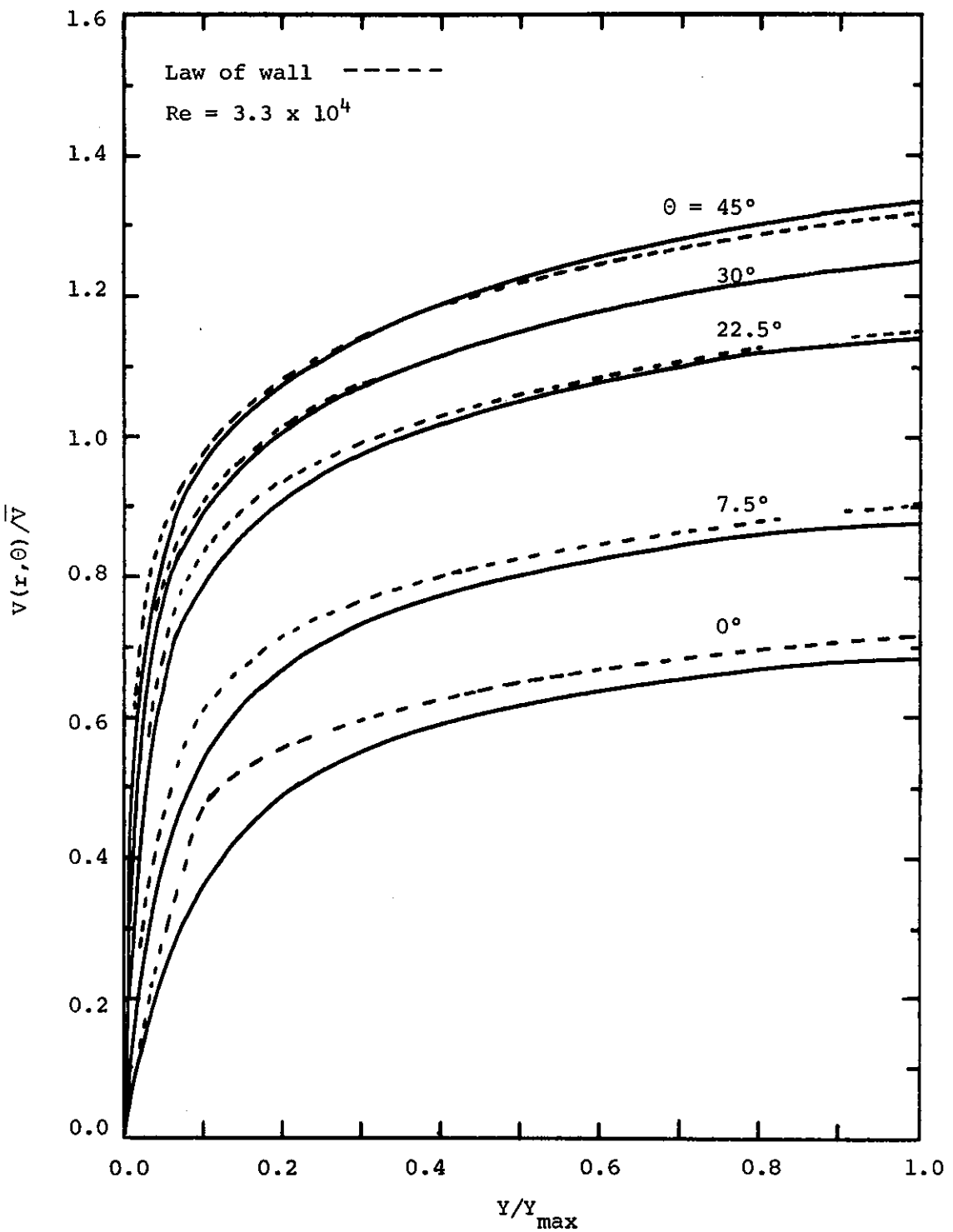

FIGURE 11(b) RADIAL VELOCITY PROFILE (p/d = 1.10)

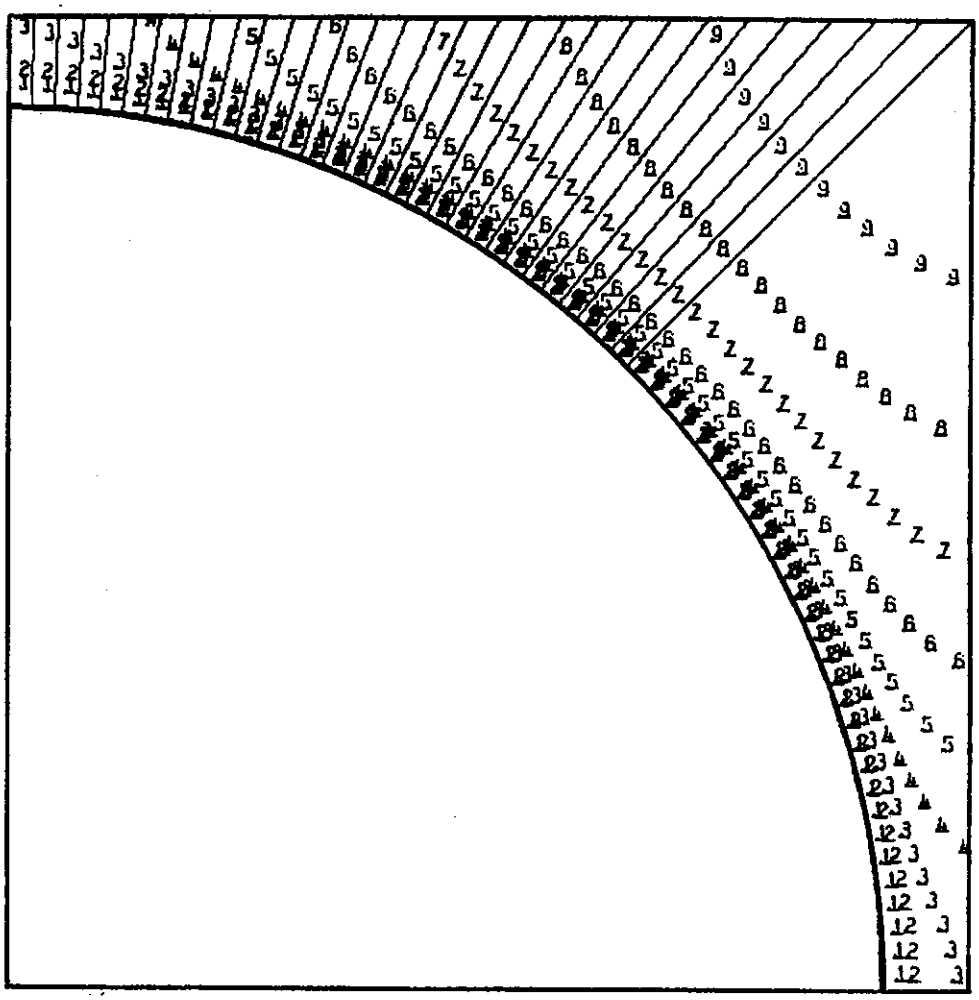

FIGURE 12. POINT INTERPOLATION OF VELOCITY FIELD

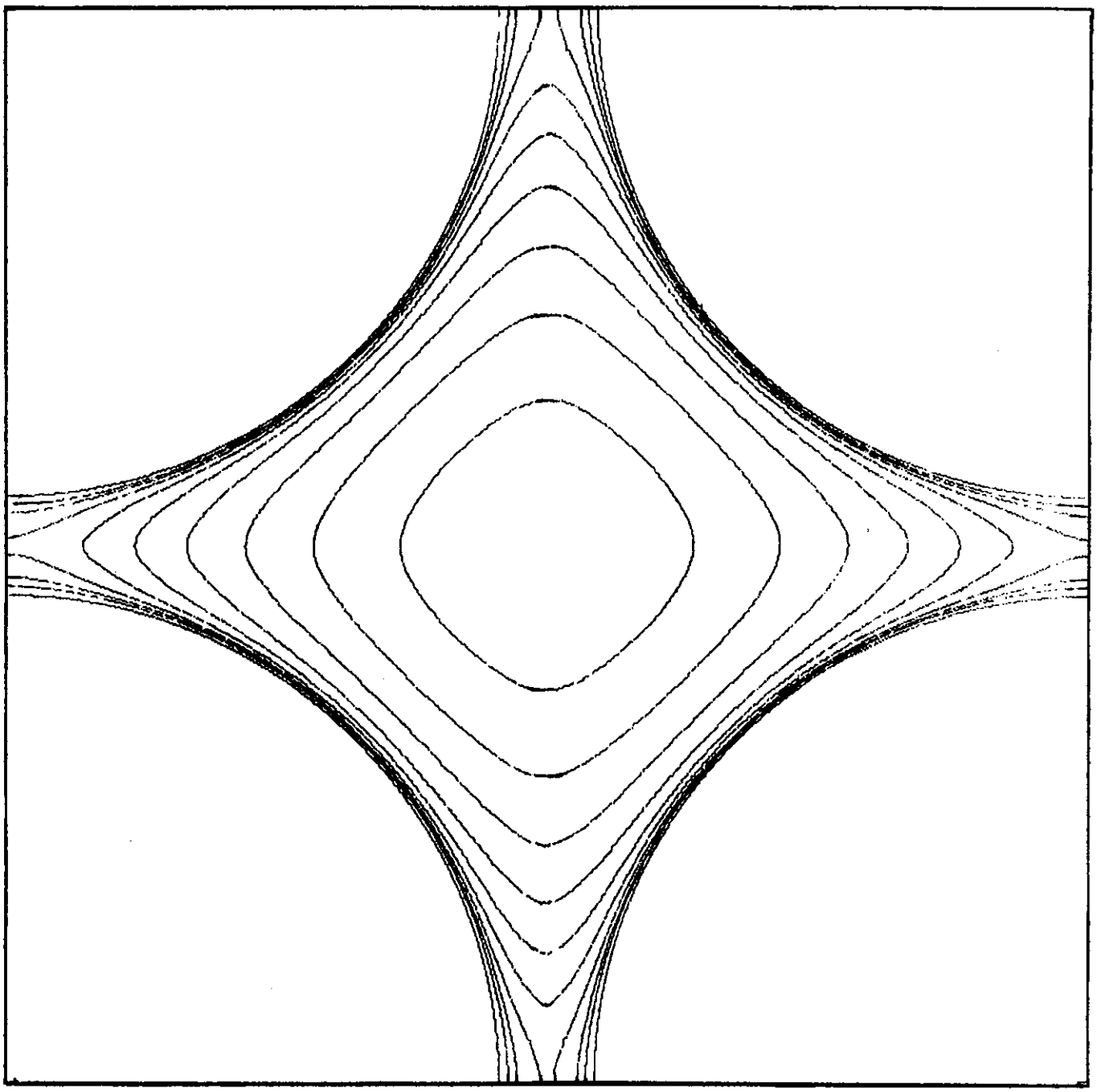

FIGURE 13. ISOTACHS FOR FOUR-ROD SUBCHANNEL (p/d) RATIO 1.10

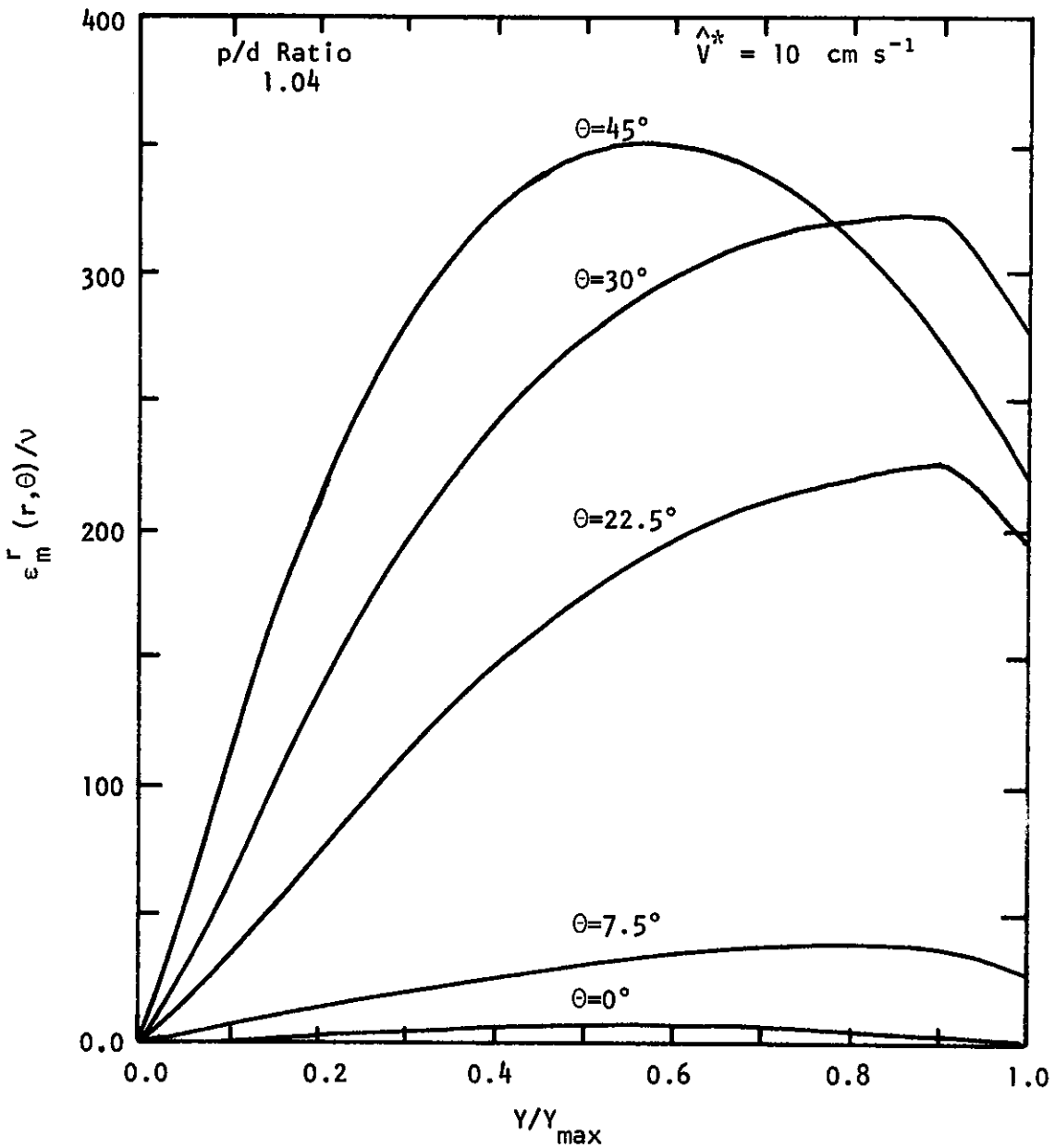

FIGURE 14(a) RADIAL EDDY MOMENTUM DIFFUSIVITY (Θ = 0 IN THE ROD GAP)

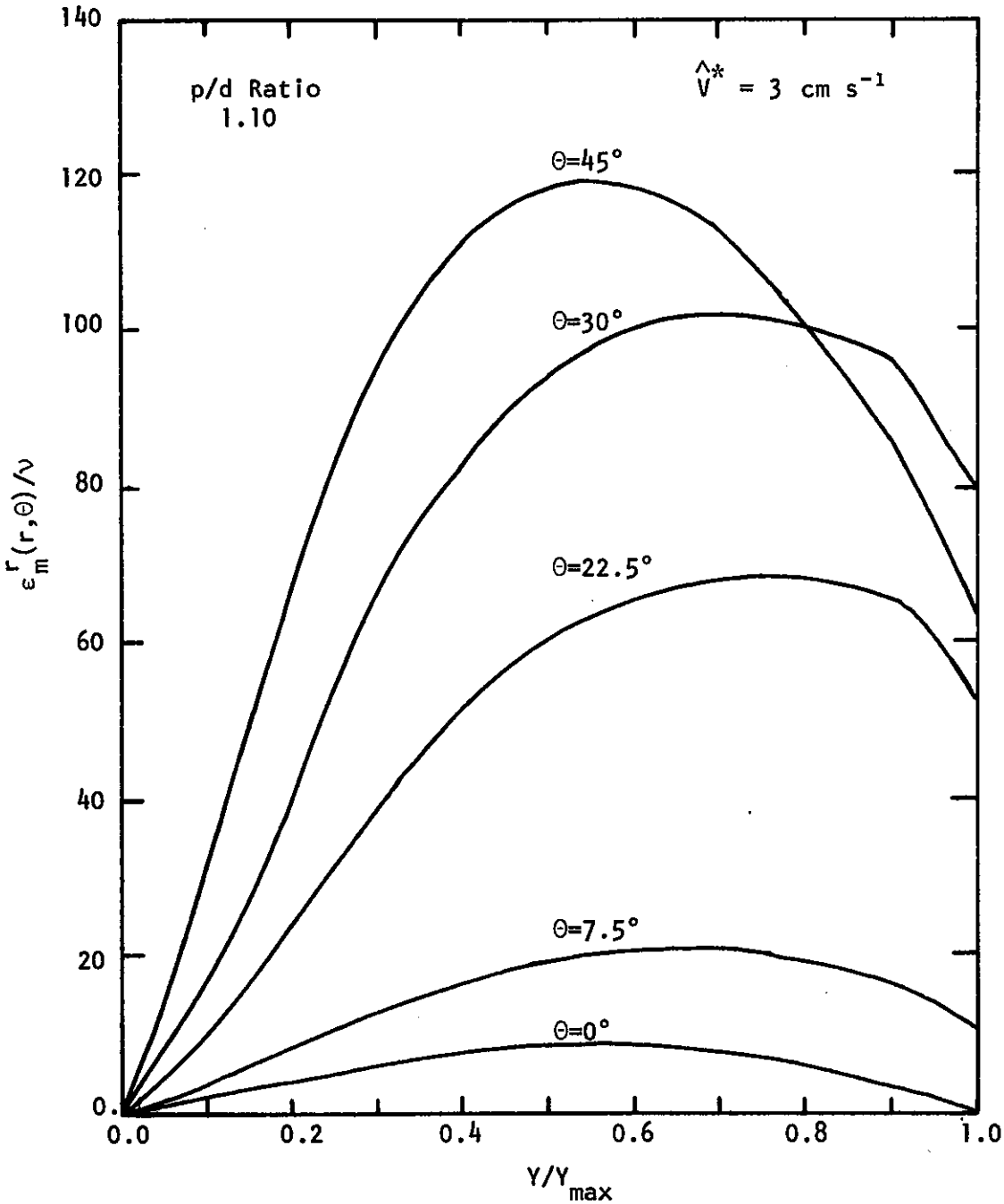

FIGURE 14(b) RADIAL EDDY MOMENTUM DIFFUSIVITY

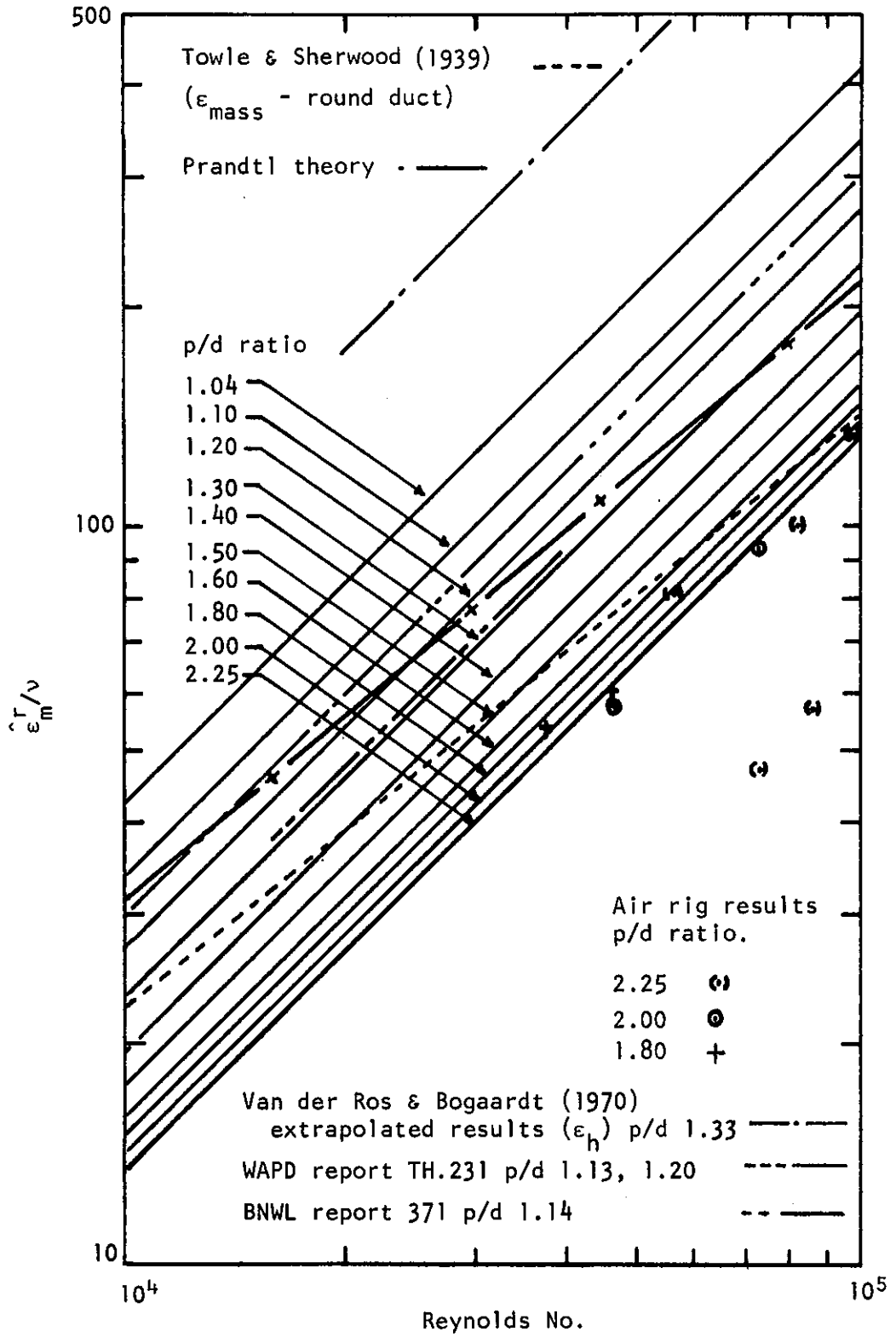

FIGURE 15. $\hat{\varepsilon}^r_m/\nu$ AS A FUNCTION OF p/d AND REYNOLDS NUMBER

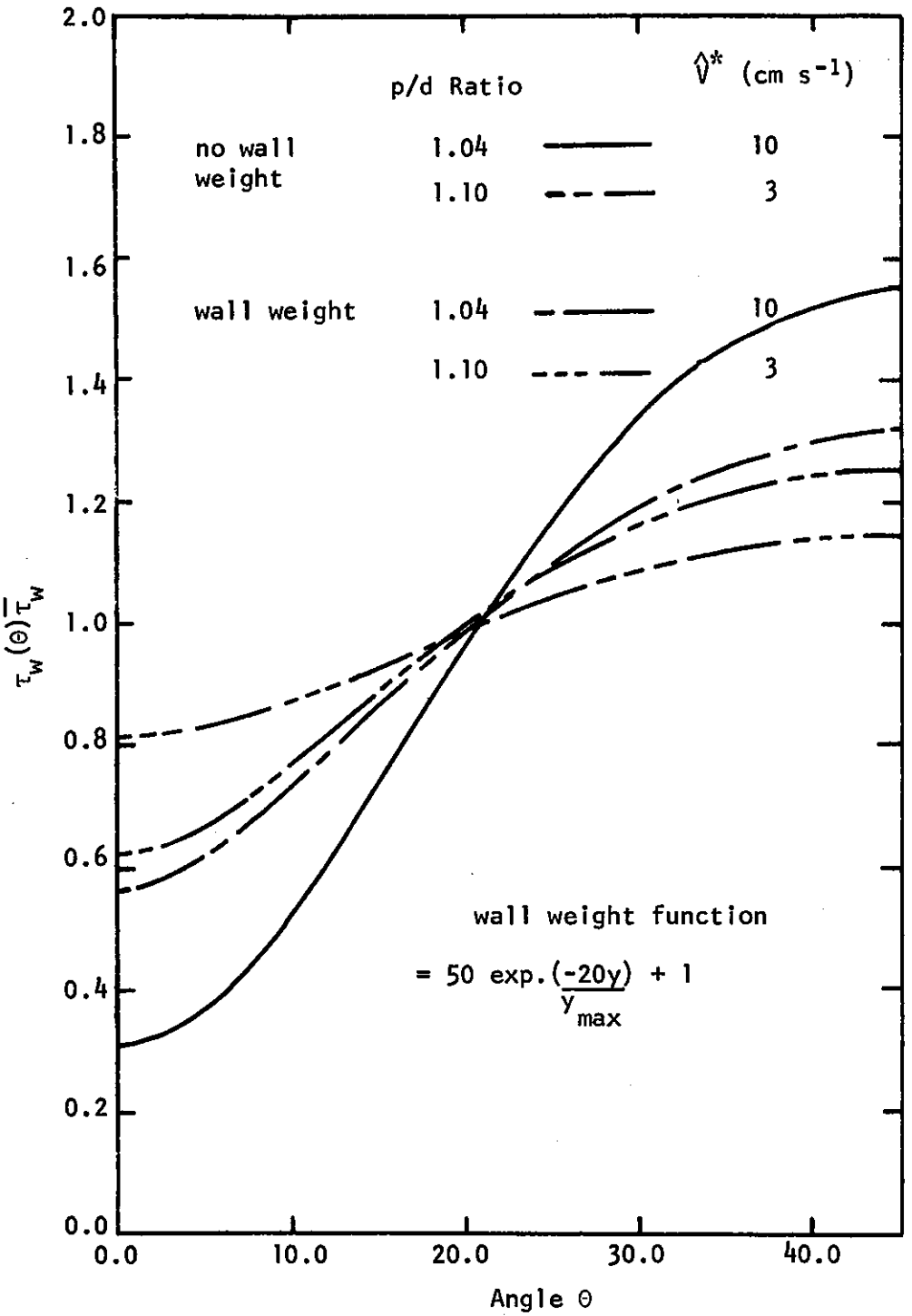

FIGURE 16. EFFECT OF ANISOTROPY OF WALL TURBULENCE ON THE WALL SHEAR STRESS DISTRIBUTION

APPENDIX A

ROFLO PROGRAM STRUCTURE

A two-loop structure is required to apply the Buleev theory to the numerical calculation of the average velocity solution of the momentum equation, and the computer program ROFLO is arranged in this basic structure, (Figure A1). The initial part of the program sets up the calculation mesh, initial velocity field and values of the total velocity gradient at eddy momentum diffusivity mesh points, using the fixed maximum value of the wall friction velocity, $\hat{V}^*$. The scale of turbulence length is calculated at each mesh point for the radial and angular eddy diffusivity coefficients and stored in matrices TR(I,J) and TA(I,J). The initial values of the eddy diffusivity are found, and the outer iteration loop of the program started. The inner loop of the program is the finite difference approximation to the momentum equation, generated by subroutine DIFF2, and this loop is then entered. The initial velocity solution is changed by the five-point difference equation until the percentage alteration in the velocity field is less than a set error limit, and the outer loop is re-entered. The new velocity gradient values are calculated, and a new set of eddy momentum diffusivity coefficients found. The diffusion approximation in the inner loop of the program is then used to find the next velocity solution, and the two-loop iterative sequence repeated until both the velocity field and eddy diffusivity values converge. The subchannel average velocity is calculated, together with the Reynolds number and friction factor.

A number of graph plotting subroutines were developed to draw the velocity solution, using the computer off-line plotter.

A1. ROFLO SUBROUTINES

A1.1 Subroutine SVEL

This subroutine sets up an initial velocity matrix based on the asymptotic law of the wall [Schlichting 1968]:

$$V^+ = 5.75 \log_{10} (y^+) + 5.50,$$

for dimensionless wall distances y^+ greater than 11.64. This value of y^+ corresponds to the intersection of the laminar sublayer equation

$$V^+ = y^+$$

and the logarithmic law of the wall. All velocity points on the same radial mesh have the same initial value.

A1.2 Subroutine TURBO and TURBO 1

Double-entry subroutine TURBO-TURBO 1 calculates the scale of turbulence length, L, at each radial and angular eddy diffusivity mesh point. The method used is shown in Section 3.2 and the scale of turbulence lengths are stored by matrices TR(I,J) and TA(I,J) for the radial and angular mesh points. A function subroutine, GEOM, called by this subroutine performs the Gaussian quadrature integration for each of the four rods.

A1.3 Subroutine SDVEL

The total velocity gradient, $|\frac{\partial \bar{V}}{\partial n}|$, is required at each radial and angular eddy diffusivity mesh point, to calculate the initial values of these quantities. The method of setting up the initial velocity field produces zero angular gradient. Consequently, the radial derivative of these equations was used by subroutine SDVEL to set the initial velocity gradients at the required mesh locations.

A1.4 Subroutines EDDYR, EDDYA

The values of the radial and angular eddy diffusivity are calculated by subroutines EDDYR and EDDYA, using an approximation to the integral developed by Buleev.

The radial eddy momentum diffusivity at a point in the fluid at which the scale of turbulence length is L_0, is given by the following integration, evaluated in the radial mesh direction:

$$\varepsilon_m^r(r,\theta) = \frac{L_0^2}{4} \int_{\frac{-1}{\delta}}^{\frac{1}{\delta}} \frac{L}{L_0} \left|\frac{\partial \bar{V}}{\partial n}\right| f_0\ (1.20\ p\ h)\ f_1(1.20\ p\ h)\ ,$$

$$0.72\ \frac{h}{\delta L_0}\ e^{-1.20\ \frac{h}{\delta L_0}}\ d\left(\frac{h}{\delta L_0}\right)\ .$$

The factor δ is a dimensionless constant used in the theory, and variable p is given by:

$$p = \frac{222\ \nu}{L^3 \left|\frac{\partial V}{\partial n}\right|}\ .$$

The attenuating functions (f_0, f_1) used by Buleev are:

$$f_0 = e^{-ph}$$

$$f_1 = \frac{1}{ph}\ (1 - e^{-ph})\ .$$

The integration is performed numerically by the following approximation:

$$\varepsilon_m^r\ (r,\ \theta) = 0.23\ L_0^2 \sqrt{\frac{4.0}{\rho} \frac{\partial p}{\partial z} \frac{1}{d_H}} \cdot \sum_{i=1}^{6} \omega_i \left|\frac{\partial \bar{V}}{\partial n}\right| f_0(p\ x_i)\ f_1(p\ x_i)\ \frac{L}{L_0}\ .$$

The values of the six weights, ω_i, and the radial distances x_i from the radial eddy diffusivity points are given in Table A1.

TABLE A1

ω_i	$\pm x_i$
0.19	0.167 L_0
0.19	0.500 L_0
0.12	0.833 L_0

The same equation applied to the angular eddy diffusivities, ε_m^θ (r, θ), with the direction of integration along the tangent to the radial mesh. The direction of integration for the angular diffusivities was approximated to integration along a constant radius line. This approximation is reasonable in the wall region, where the tangential path of integration is closely approximated by the short radial path, and it is in this wall region that experimental results suggest a significant difference between the angular and radial diffusivities.

In the laminar sublayer region, the eddy momentum diffusivities decay to zero, and the magnitude of the variable p_1 used by the attenuating functions f_0 and f_1 becomes large. To avoid underflow problems in evaluating these functions by the function subroutine AFCT, the attenuating functions become zero if the absolute value of the argument exceeds thirty.

A1.5 Subroutines RGDT1, RGDT2, RGDT3

The total velocity gradient at the radial eddy diffusivity mesh points is evaluated by these subroutines.

The radial velocity component of the total velocity gradient is found in terms of the two bounding radial velocity points. An average of four angular gradients is used to define the angular velocity gradient, these four gradients being determined by the six surrounding velocity points (Figure 4).

A1.6 Subroutine AGDT1

The total velocity gradient at the angular eddy momentum diffusivity mesh points is evaluated by subroutine AGDT1. The angular velocity gradient is evaluated from the two bounding radial velocity points (Figure 4). An average of the four surrounding radial velocity gradients is used to determine the radial velocity gradient at this mesh point.

A1.7 Subroutine DIFF2

The finite difference approximation to the momentum equation is generated by subroutine DIFF2, using the latest estimates of the radial and angular eddy

diffusivity values. The first half of the subroutine recalculates the magnitude of the four coupling coefficients linking each velocity point to the four surrounding velocity values, and these corrected coefficients are stored in four matrices. The second half of the subroutine iteratively solves for the average velocity field, using a finite difference approximation developed from Equation (16). The extrapolated Liebmann method is used, with a value of the extrapolation parameter, Ω, set at 1.7. The optimum magnitude of the extrapolation parameter could not be found by theoretical methods, and a trial and error process was used to set this value.

The iterative process is continued until the maximum percentage difference between successive values of the velocity, at any point in the mesh, is less than a pre-set maximum error. If the velocity iteration loop fails to converge to the required accuracy within a set number of iterations, this loop is terminated and new values of the eddy diffusivity are calculated by the outer loop in the main program.

However, if sufficient angular mesh points are used, the velocity iteration converges before exceeding this number of iterations.

The percentage error limit used to determine the convergence of the velocity field was 0.25 per cent, and the limit to the number of velocity iterations was normally set at 100.

A1.8 Subroutine VAVER

The subchannel average velocity is calculated by subroutine VAVER, after the convergence of both the eddy diffusivity values and the average velocity field. The velocity distribution is then normalised by dividing by this average, and the subchannel Reynolds number is found.

A1.9 Subroutine FIND

The print-out of the velocity field in tabulated form for each velocity mesh point is difficult to interpret, particularly because of the non-linear mesh spacing. Several subroutines were therefore developed to draw constant velocity contours in the subchannel, using the computer-controlled Calcomp off-line plotter.

Subroutine FIND locates the radial wall distance for up to twelve velocity contour lines, at each of the N angular mesh lines.

These contours are spaced at equal velocity increments, and the radial distances are found by linear interpolation from the velocity field. The first velocity contour is determined by a point on the last angular mesh line, at a wall distance of one twentieth of the rod-gap dimension. The last velocity contour is reduced to a point, located at the subchannel centre.

A1.10 Subroutine VPLOT

A point plot of the twelve velocity contours is generated by subroutine VPLOT, for one quarter of the subchannel area. The calculation mesh area is shown by the angular mesh lines drawn in this part of the subchannel, and the velocity points are reflected from this area into the lower half of the subchannel quadrant.

A1.11 Subroutine FPLOT

A smooth curve was fitted through the velocity contour points for one half of the subchannel area, using a spline curve fit. Subroutine FPLOT reflects the velocity points of Figure 12 into the second quadrant of the subchannel, and a quadratic curve is used to join successive pairs of the points. The coefficients of the quadratic are set by subroutine SPLIC such that the first and second derivatives of the velocity contour lines are held constant at each plotted velocity point. Subroutine GPDRAW, and function subroutines CIRCL and SMOOV are called by this subroutine to control the plotter.

A3. CONVERGENCE CRITERIA AND INSTABILITY PROBLEMS

The criteria used for the convergence of the velocity program (ROFLO) was the requirement that there should be only one iteration in the velocity field calculation, after the eddy momentum diffusivity values had been changed by the outer loop in the main program. A table of the outer iteration loop number, with the number of iterations required to reach convergence in the diffusion equation subroutine DIFF2 is printed, together with the maximum change for any velocity point during the last iteration.

In the development of the program, an instability due to the interaction between the eddy diffusivity values and the magnitude of the average velocity field was found.

The initial value of the eddy diffusivity coefficients greatly reduced the magnitude of the initial velocity field, and the subsequent set of eddy diffusivity values calculated by the outer loop of the program were also reduced in magnitude. The magnitude of the velocity field calculated by these coefficients was larger than the initial velocity field, and the program oscillated between low eddy diffusivity values leading to a high-magnitude velocity solution and the reverse. This problem was corrected by averaging the new set of eddy diffusivity values with the previous set before re-entering the diffusion calculation for the average velocity distribution.

The number of angular subdivisions, N, and consequently the spacing of the radial mesh also influenced the convergence of the program. For the

error limit specified in subroutine DIFF2, it was found that with values of N less than 25 the calculation mesh generated was too coarse to allow the convergence of the velocity distribution. The maximum value of N is set at 40 by the dimension specification of the variables in the program, but a value of 30 was found to generate stable solutions of the velocity field for a range of rod pitch to diameter ratios of 2.0 to 1.05. This value of N located at least three velocity points in the radial mesh within the laminar sublayer region of the fluid, where the eddy diffusivity terms are effectively zero.

A4. MAIN ROFLO VARIABLES

VEL(80,40)	velocity distribution
DVR(80,40)	radial velocity gradient
DVA(80,40)	angular velocity gradient
EMR(80,40)	eddy momentum diffusivity (radial)
EMA(80,40)	eddy momentum diffusivity (angular)
ER(80)	radial mesh spacing
EA(80)	radial velocity mesh
OA	angular mesh
N	number of angular mesh points
DR	rod diameter (d)
VST	maximum wall friction velocity ($\hat{V}^*$)
GD	rod pitch/diameter ratio (p/d)
VIS	fluid viscosity (ν)
DE	equivalent hydraulic diameter (d_H)
PPD	axial pressure drop
OM	finite difference extrapolation parameter (Ω)
ERROR	maximum percentage difference in velocity distribution/ iteration.

A5. INPUT DATA

Two cards are used to specify the input data to the program

CARD 1: FORMAT [I10, 3F10.5, F10.8]

VARIABLES

N	angular mesh spacing ($N \leqslant 39$)
DR	rod diameter (d)
VST	maximum wall friction velocity ($\hat{V}^*$)
GD	(p/d) ratio
VIS	fluid viscosity (ν)

CARD 2: FORMAT [4F10.5]

ACOEF	weighting function for scale of turbulence length (normally = 0)
BCOEF	weighting function in Equation (37) (normally 50)
COFF	exponent in Equation (37) (normally 40)
DRAW	control variable for plotter (1 for plots, 0 for no plot).

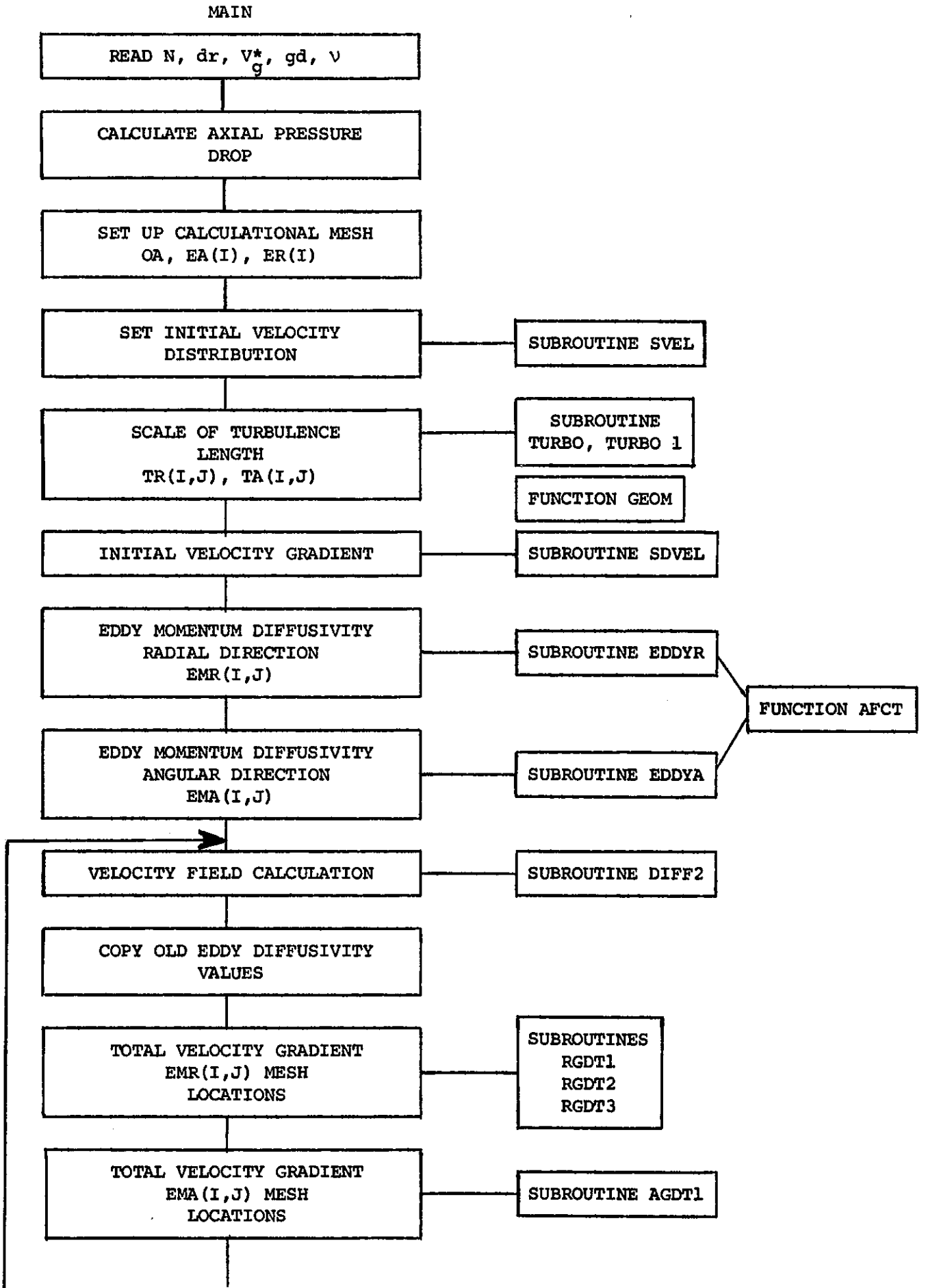

FIGURE A1. ROFLO PROGRAMME STRUCTURE

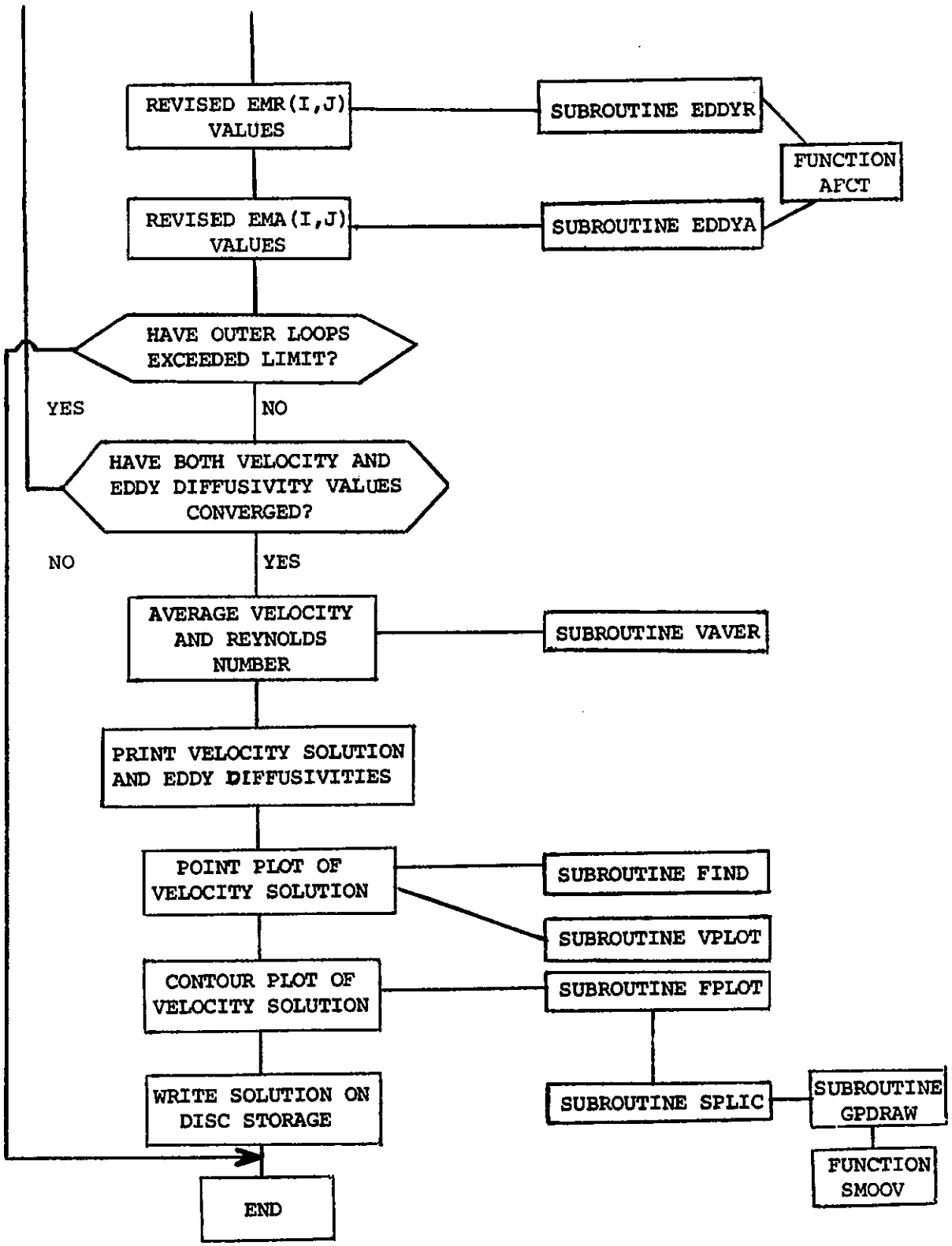

FIGURE A1. CONTINUED

APPENDIX B

ANALYTIC SOLUTION IN LAMINAR FLOW, TO SHOW EFFECT OF INTER-GAP BOUNDARY

An approximate analytic solution to the momentum equation for laminar flow within the four-rod subchannel can be found by using a bipolar coordinate system, and solving for the velocity distribution between two of the rods (Figure B1). This analytic solution can be used to show the effect of a wall between the rods in the array on the velocity distribution in a closed and open subchannel (Figure 5b).

For the infinite rod array, the laminar flow form of the momentum equation is:

$$\nabla^2 V_\infty(x, y) + C_0 = 0 \quad ,$$

and, for the closed subchannel,

$$\nabla^2 V_s(x, y) + C_1 = 0 \quad .$$

Let $$\phi = \frac{V_\infty}{C_0} - \frac{V_s}{C_1}$$

and the above equations become the Laplace equation:

$$\nabla^2 \phi = 0 \quad .$$

The boundary conditions for ϕ are 0 on the rod surface, and $(V_\infty/C_0)\big|_{x=0}$ on the wall between the rods (y axis).

Transforming to bipolar coordinates (ξ, θ), the equation becomes

$$\frac{\partial^2 \phi}{\partial \xi^2} + \frac{\partial^2 \phi}{\partial \phi^2} = 0 \quad .$$

with $$x = \frac{a \sin \theta}{\cosh \xi + \cos \theta}$$

and $$y = \frac{a \sinh \xi}{\cosh \xi + \cos \theta} \quad .$$

The pitch to diameter ratio is:

$$1 + \alpha = \frac{a \coth \xi_0}{a \operatorname{cosech} \xi_0}$$

and the wall gap

$$g = \frac{2a\alpha}{\sqrt{\alpha^2 + 2\alpha}} \quad .$$

Hence along the centreline,

$$\frac{x}{g} = \frac{\sin\theta}{2(1+\cos\theta)}\sqrt{1+2/\alpha}$$

The solution of the Laplace equation for ϕ is:

$$\phi = \sum_{i=1}^{\infty} A_i e^{-\lambda_i \theta} \cos \lambda_i \xi \quad .$$

As ϕ is zero on the rod surface (ξ_0)

$$\lambda_i = (2_i - 1)\frac{\pi}{2\xi_0}$$

and so

$$\sum_{i=1}^{\infty} A_i \cos \lambda_i \xi = \frac{V_\infty}{C_0}\Big|_{\xi=0}$$

for the x axis.

The difference between the infinite rod array velocity solution to the solution for a wall in the rod gap, along the x axis, is defined as the error (ε):

$$\varepsilon = \left(\frac{V_\infty}{C_0} - \frac{V_s}{C_1}\right)/\frac{V_\infty}{C_0}\Big|_{0,\theta}$$

$$= \phi/\frac{V_\infty}{C_0}\Big|_{0,\theta} \quad .$$

Taking only the first term of the series for ϕ, the error becomes

$$\varepsilon \doteq e^{-\pi\theta/2\xi_0}$$

with

$$\xi_0 = \cosh^{-1}(1+\alpha)$$

and θ determined for each (x/g) ratio.

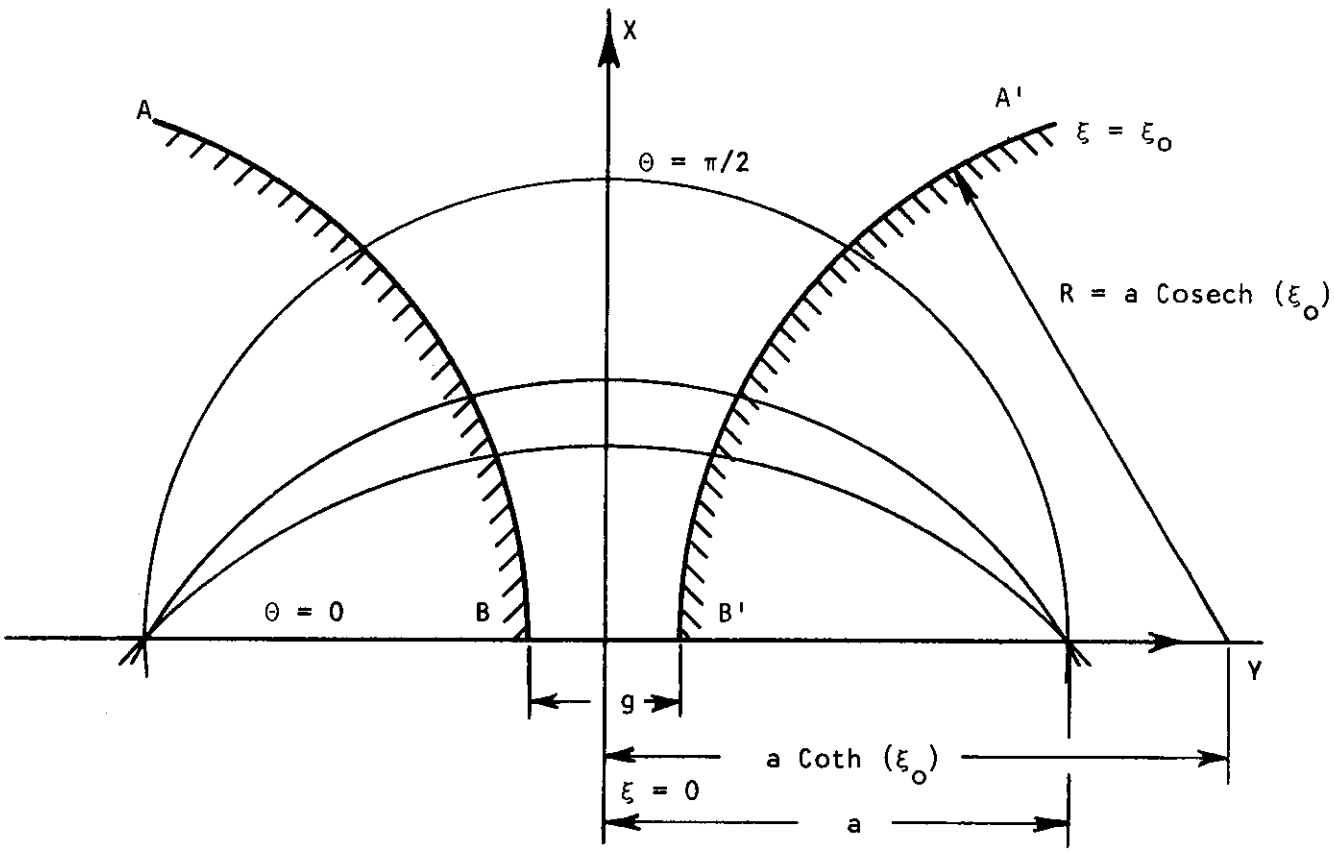

g = Gap width

R - Rod radius

FIGURE B1. BIPOLAR CO-ORDINATE SOLUTION OF THE LAMINAR VELOCITY DISTRIBUTION IN THE FLOW AREA ABB́Á